

Characterizing the companion AGBs using surface chemical composition of barium stars ^{*}

J. Shejeelammal¹, Aruna Goswami¹, Partha Pratim Goswami¹,
Rajeev Singh Rathour^{1,2}, Thomas Masseron^{3,4}

¹ *Indian Institute of Astrophysics, Koramangala, Bangalore 560034, India; aruna@iiap.res.in*

² *Indian Institute of Science Education and Research, Pune, Maharashtra 411008, India*

³ *Instituto de Astrofísica de Canarias, E-38205 La Laguna, Tenerife, Spain*

⁴ *Departamento de Astrofísica, Universidad de La Laguna, E-38206 La Laguna, Tenerife, Spain.*

Accepted —; Received —; in original form —

ABSTRACT

Barium stars are one of the important probes to understand the origin and evolution of slow neutron-capture process elements in the Galaxy. These are extrinsic stars, where the observed s-process element abundances are believed to have an origin in the now invisible companions that produced these elements at their Asymptotic Giant Branch phase of evolution. We have attempted to understand the s-process nucleosynthesis, as well as the physical properties of the companion stars through a detailed comparison of observed elemental abundances of 10 barium stars with the predictions from AGB nucleosynthesis models, FRUITY. For these stars, we have presented estimates of abundances of several elements, C, N, O, Na, Al, α -elements, Fe-peak elements and neutron-capture elements Rb, Sr, Y, Zr, Ba, La, Ce, Pr, Nd, Sm and Eu. The abundance estimates are based on high resolution spectral analysis. Observations of Rb in four of these stars have allowed us to put a limit to the mass of the companion AGB stars. Our analysis clearly shows that the former companions responsible for the surface abundance peculiarities of these stars are low-mass AGB stars. Kinematic analysis have shown the stars to be members of Galactic disk population.

Key words: stars: Abundances - stars: chemically peculiar - stars: nucleosynthesis - stars: individual

1 INTRODUCTION

Understanding the nucleosynthesis and evolution of Asymptotic Giant Branch (AGB) stars are of primary importance as they are the major factories of some key elements in the Universe (Busso et al. 1999, Herwig 2005). They are the predominant sites for the slow neutron-capture nucleosynthesis, and major contributors of elements heavier than iron; upto half of all the heavy elements are produced through s-process (Busso et al. 1999). There are certain isotopes like ⁸⁶Sr, ⁹⁶Mo, ¹⁰⁴Pd, ¹¹⁶Sn etc., which are known to be produced only through the s-process. It has been estimated that a third of the total carbon content in the Galaxy is produced in AGB stars, which is about the same amount as produced in CCSNe and Wolf-Rayet stars (Dray et al. 2003). Besides these, the intermediate-mass AGB stars are the major producers of ¹⁴N in the Galaxy (Henry et al. 2000, Merle et al. 2016).

The exact physical conditions and nucleosynthetic processes occurring at the interior of AGB stars are not clearly understood that hinders a better understanding of the contribution of these stars to the Galactic chemical enrichment. This demands a need for detailed chemical composition studies for an extended sample of AGB stars. However, the spectra of the AGB stars are complicated as it is overwhelmed with the molecular contributions arising due to their low photospheric temperature. This makes the derivation of exact elemental abundance difficult. In this regard, the extrinsic stars, which are known to have received products of AGB phase of evolution via binary mass transfer mechanisms, form vital tools to trace the AGB nucleosynthesis. The important classes of such extrinsic stars are barium stars as the analysis of their generally hotter spectra is more accurate (Bidelman & Keenan 1951), CH stars (Keenan 1942) and CEMP-s stars (Beers & Christlieb 2005). Most of them are radial velocity variables (McClure et al. 1980, McClure 1983, 1984, McClure & Woodsworth 1990, Udry et al. 1998a,b, Lucatello et al. 2005) associated with a now invisible white dwarf companion.

^{*} Based on data collected using HCT/HESP, UVES and FEROS

Detailed studies on barium stars include Allen & Barbay (2006a), Smiljanic et al. (2007), de Castro et al. (2016), Yang et al. (2016) and many others. However, these studies have not included abundances of several heavy elements such as Rb for all the stars and also for C, N and O. In this work, we have undertaken to carry out a detailed spectroscopic analysis for a sample of ten barium/CH star candidates and derived whenever possible the abundances of C, N, O and the neutron density dependent [Rb/Zr] abundance ratio to investigate the neutron source in the former companion AGB stars. There are two important neutron sources for the s-process in the He intershell of AGB stars: $^{13}\text{C}(\alpha, n)^{16}\text{O}$ reaction during the radiative inter-pulse period and $^{22}\text{Ne}(\alpha, n)^{25}\text{Mg}$ reaction during the convective thermal pulses. $^{13}\text{C}(\alpha, n)^{16}\text{O}$ reaction is the dominant neutron source in low-mass AGB stars with initial mass $\leq 3 M_{\odot}$. The temperature $T \geq 90 \times 10^6$ K required for the operation of this reaction provides a neutron density $N_n \sim 10^8 \text{ cm}^{-3}$ in a timescale of $\geq 10^3$ years (Straniero et al. 1995, Gallino et al. 1998, Goriely & Mowlavi 2000, Busso et al. 2001). A temperature 300×10^6 K, required for the activation of ^{22}Ne source is achieved during the TPs in intermediate-mass AGB stars (initial mass $\geq 4 M_{\odot}$). It produces a neutron density $N_n \sim 10^{13} \text{ cm}^{-3}$ in a timescale of ~ 10 years. The temperature required for the ^{22}Ne source is reached in low-mass stars during the last few TPs providing $N_n \sim 10^{10} - 10^{11} \text{ cm}^{-3}$ (Iben 1975, Busso et al. 2001). The Rb is produced only when the $N_n > 5 \times 10^8 \text{ cm}^{-3}$, otherwise Sr, Y, Zr etc. are produced. Hence, the [Rb/Zr] ratio can be used as an indicator of mass of AGB stars. We could determine Rb abundance in four of our program stars; HD 32712, HD 36650, HD 179832 and HD 211173.

In section 2, we describe the source of the spectra used in this study. Section 3 describes the methodology used for the determination of atmospheric parameters, elemental abundances and radial velocities. A discussion on the stellar mass determination is also provided in the same section. A comparison of our result with the literature values are presented in section 3. In section 4, we discuss the procedures adopted for the abundance determination of different elements. Section 5 provides a discussion on abundance uncertainties. Section 6 provides the discussion on the elemental abundance ratios and their interpretations based on the existing nucleosynthesis theories. This section also provides a comparison of the observational data with the FRUITY models of Cristallo et al. (2009, 2011, 2015b) and a parametric model based analysis. A discussion on the individual stars are also given in the same section. Conclusions are drawn in section 7.

2 OBJECT SELECTION, DATA ACQUISITION AND DATA REDUCTION

The objects analyzed in this study are taken from the CH star catalog of Bartkevicius (1996). Six of them are also found listed in the barium star catalog of Lü (1991). These stars lie among the typical CH stars in the color magnitude ((B-V) v/s MV) diagram. The spectra of these objects are acquired from three different sources. For HD 219116, HD 154276 and HD 147609, the high resolution spectra ($\lambda/\delta\lambda \sim 60,000$) were obtained on October 2015, May

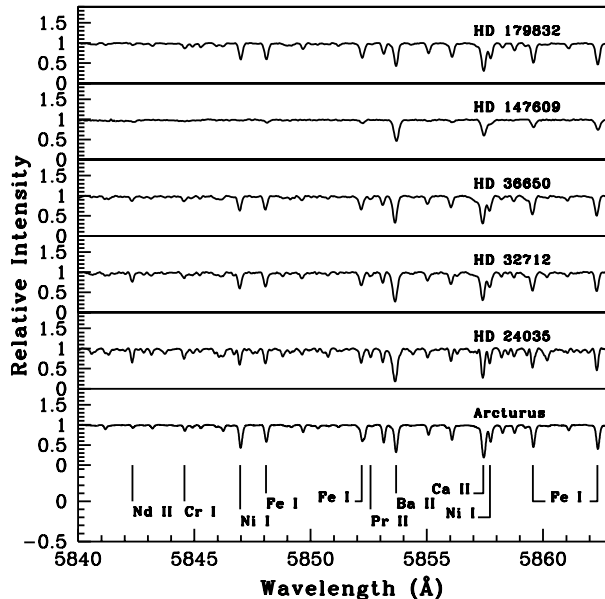


Figure 1. Sample spectra of the program stars in the wavelength region 5840 to 5863 Å.

2017 and June 2017 using the high resolution fiber fed Hanle Echelle SPectrograph (HESP) attached to the 2m Himalayan Chandra Telescope (HCT) at the Indian Astronomical Observatory, Hanle. The wavelength coverage of the HESP spectra spans from 3530 - 9970 Å. The Data are reduced following the standard procedures using various tasks in Image Reduction and Analysis Facility (IRAF¹) software. For HD 24035 and HD 207585 high resolution spectra ($\lambda/\delta\lambda \sim 48,000$) are obtained with the UVES (Ultraviolet and Visual Echelle Spectrograph) of the 8.2m Very Large Telescope (VLT) of ESO at Cerro Paranal, Chile. A high resolution spectrum of HD 219116 is also obtained from UVES/VLT. The wavelength coverage of the UVES spectra spans from 3290 - 6650 Å. For HD 32712, HD 36650, HD 94518, HD 211173 and HD 179832, high resolution spectra ($\lambda/\delta\lambda \sim 48,000$) are obtained with the FEROS (Fiber-fed Extended Range Optical Spectrograph) of the 1.52 m telescope of ESO at La Silla, Chile. The wavelength coverage of the FEROS spectra spans from 3520 - 9200 Å. Basic data of the program stars along with the source of spectra are given in the Table 1. A few sample spectra are shown in Figure 1.

3 STELLAR ATMOSPHERIC PARAMETERS AND RADIAL VELOCITY ESTIMATION

We have estimated the photometric temperature of the program stars using the temperature calibration equations of Alonso et al. (1994, 1996) for dwarfs and Alonso et al. (1999, 2001) for giants, and following the detailed procedures as

¹ IRAF is distributed by the National Optical Astronomical Observatories, which is operated by the Association for Universities for Research in Astronomy, Inc., under contract to the National Science Foundation

Table 1. Basic data for the program stars.

Star	RA(2000)	Dec.(2000)	B	V	J	H	K	Exposure (seconds)	Date of obs.	Source of spectrum
HD 24035	03 43 42.53	-72 36 32.80	9.74	8.51	6.567	6.043	5.919	900	05/04/2002	UVES
HD 32712	05 01 34.91	-58 31 15.05	9.71	8.55	6.634	6.054	5.912	1200	11/11/1999	FEROS
HD 36650	05 27 42.92	-68 04 27.16	9.91	8.79	6.812	6.297	6.190	1200	10/11/1999	FEROS
HD 94518	10 54 12.20	-31 09 34.58	8.95	8.36	7.182	6.891	6.824	900	02/01/2000	FEROS
HD 147609	16 21 51.99	+27 22 27.19	9.69	9.18	8.211	8.035	7.948	2400(3)	01/06/2017	HESP
HD 154276	17 03 49.15	+17 11 21.08	9.80	9.13	7.911	7.624	7.549	2400(3)	06/05/2017	HESP
HD 179832	19 16 30.00	-49 13 13.01	9.46	8.44	6.660	6.163	6.031	600	14/07/2000	FEROS
HD 207585	21 50 34.71	-24 11 11.68	10.50	9.78	8.633	8.341	8.301	240	24/04/2002	UVES
HD 211173	22 15 57.01	-31 51 38.52	9.43	8.49	6.810	6.332	6.218	600	14/07/2000	FEROS
HD 219116	23 13 30.24	-17 22 08.71	10.29	9.25	7.602	7.137	7.012	240 2400(3)	19/05/2002 30/10/2015	UVES HESP

The numbers in the parenthesis with exposures indicate the number of frames taken.

described in our earlier papers (Goswami et al. 2006, 2016). We made use of the 2MASS J, H, K magnitudes taken from SIMBAD (Cutri et al. 2003) for this calculation. The photometric temperature estimates had been used as an initial guess for deriving the spectroscopic effective temperature of each object.

To determine the stellar atmospheric parameters, we have used a set of clean, unblended Fe I and Fe II lines with excitation potential in the range 0.0 - 6.0 eV and equivalent width 20 - 180 mÅ. IRAF software is used for the equivalent width measurement. A pseudo continuum (at 1) is fitted to the observed spectrum using the spline function. The equivalent width is measured for each spectral line by fitting a Gaussian profile. An initial model atmosphere was selected from the Kurucz grid of model atmosphere with no convective overshooting (<http://cfaku5.cfa.harvard.edu/>) using the photometric temperature estimate and the guess of log g value for giants/dwarfs. A final model atmosphere was adopted by the iterative method from the initially selected one, using the most recent version of the radiative transfer code MOOG (Snedden 1973) based on the assumptions of Local Thermodynamic Equilibrium (LTE).

The effective temperature is determined by the method of excitation equilibrium, forcing the slope of the abundances from Fe I lines versus excitation potentials of the measured lines to be zero. The micro-turbulent velocity at a fixed effective temperature is determined by demanding that there will be no dependence of the derived Fe I abundance on the reduced equivalent width of the corresponding lines. Micro-turbulent velocity is fixed at a value which gives zero slope for the plot of equivalent width versus abundances of Fe I lines. The surface gravity, log g value is determined by means of ionization balance, that is by forcing the Fe I and Fe II lines to produce the same abundance at the selected effective temperature and microturbulent velocity. The estimated abundances from Fe I to Fe II lines as a function of excitation potential and equivalent widths, respectively, are shown in figures that are made available as on-line materials.

A comparison of our results with the literature values whenever available shows a close match well within the error limits.

Radial velocities of the program stars are calculated using a set of clean and unblended lines of several elements. In Table 2 we present the derived atmospheric parameters

and radial velocities of the program stars. Our radial velocity estimates are used to study the kinematic properties of the stars. A table giving the results from kinematic analysis is presented in the Appendix (Table 14). Three objects in our sample, HD 24035, HD 147609 and HD 207585 are confirmed binaries with orbital periods of 377.83 ± 0.35 days (Udry et al. 1998a), 672 ± 2 days (Escorza et al. 2019), and 1146 ± 1.5 days (Escorza et al. 2019) respectively. Our estimated radial velocity (-1.56 km^{-1}) for HD 24035 is slightly higher than the range of radial velocities found in literature (-2.14 to -19.81) for this object. However, for HD 207585 (-65.9 km^{-1}) and HD 147609 (-18.17 km^{-1}), our estimates fall well within the range of velocities available in literature, i.e., (-52.2 to -74.1) and (-19.2 to -11.9) respectively.

We have determined the mass of the program stars from their location in Hertzsprung-Russell diagram (Girardi et al. 2000 data base of evolutionary tracks) using the spectroscopic temperature estimate, T_{eff} , and the luminosity, $\log(L/L_{\odot})$.

$$\log(L/L_{\odot}) = 0.4(M_{\text{bol}\odot} - V - 5 - 5 \log(\pi) + A_V - BC)$$

The visual magnitudes V are taken from Simbad and the parallaxes

π from Gaia DR2 (<https://gea.esac.esa.int/archive/>). The bolometric correction, BC, is calculated using the empirical calibrations of Alonso et al. (1995) for dwarfs and Alonso et al. (1999) for giants. The interstellar extinction A_V is calculated using the calibration equations given in Chen et al. (1998). From the estimated mass, log g is calculated using $\log(g/g_{\odot}) = \log(M/M_{\odot}) + 4 \log(T_{\text{eff}}/T_{\text{eff}\odot}) - \log(L/L_{\odot})$. We have adopted the solar values $\log g_{\odot} = 4.44$, $T_{\text{eff}\odot} = 5770\text{K}$ and $M_{\text{bol}\odot} = 4.74$ mag.

We have used $z = 0.004$ tracks for HD 24035 and HD 94518; $z = 0.008$ for HD 207585 and HD 219116; $z = 0.019$ for HD 32712, HD 36650, HD 147609, HD 154276 and HD 211173, and $z = 0.030$ for HD 179832. As an example, the evolutionary tracks for a few objects are shown in Figure 2. The mass estimates are presented in Table 3.

4 ABUNDANCE DETERMINATION

Abundances of most of the elements are determined from the measured equivalent width of lines of the neutral and ionized atoms using the most recent version of MOOG and the adopted model atmospheres. Absorption lines corresponding

Table 2. Derived atmospheric parameters for the program stars.

Star	T_{eff} (K) ± 100	$\log g$ cgs ± 0.2	ζ (km s^{-1}) ± 0.2	[Fe I/H]	[Fe II/H]	V_r (km s^{-1})	V_r (km s^{-1})
HD 24035	4750	2.20	1.58	-0.51 ± 0.19	-0.50 ± 0.16	-1.56 ± 0.25	-12.51 ± 0.13
HD 32712	4550	2.53	1.24	-0.25 ± 0.12	-0.25 ± 0.12	$+10.37 \pm 0.02$	$+11.27 \pm 0.16$
HD 36650	4880	2.40	1.30	-0.02 ± 0.12	-0.02 ± 0.14	$+36.40 \pm 0.19$	$+31.52 \pm 0.47$
HD 94518	5700	3.86	1.30	-0.55 ± 0.10	-0.55 ± 0.12	$+92.20 \pm 0.43$	92.689 ± 0.015
HD 147609	6350	3.50	1.55	-0.28 ± 0.16	-0.28 ± 0.12	-18.17 ± 1.47	-17.11 ± 0.82
HD 154276	5820	4.28	0.63	-0.09 ± 0.13	-0.10 ± 0.14	-64.17 ± 1.42	-55.94 ± 0.17
HD 179832	4780	2.70	0.99	$+0.23 \pm 0.04$	$+0.22 \pm 0.06$	$+6.73 \pm 0.03$	$+7.64 \pm 0.13$
HD 207585	5800	3.80	1.00	-0.38 ± 0.12	-0.38 ± 0.11	-65.97 ± 0.07	-60.10 ± 1.20
HD 211173	4900	2.60	1.15	-0.17 ± 0.10	-0.17 ± 0.09	-27.84 ± 0.25	-28.19 ± 0.63
HD 219116	5050	2.50	1.59	-0.45 ± 0.11	-0.44 ± 0.11	-40.90 ± 0.25	-11.00 ± 7.30

In Columns 7 and 8 we present radial velocities from the respective spectra and SIMBAD respectively

Table 3. Estimates of $\log g$ and Mass using parallax method

Star name	Parallax (mas)	M_{bol}	$\log(L/L_{\odot})$	Mass(M_{\odot})	$\log g$ (cgs)	$\log g$ (spectroscopic) (cgs)
HD 24035	4.612 ± 0.101	1.401 ± 0.05	1.339 ± 0.02	0.70 ± 0.21	2.61 ± 0.02	2.20
HD 32712	2.621 ± 0.026	0.081 ± 0.022	1.868 ± 0.01	1.80 ± 0.26	2.41 ± 0.005	2.53
HD 36650	2.655 ± 0.027	0.474 ± 0.023	1.710 ± 0.01	2.20 ± 0.26	2.78 ± 0.01	2.40
HD 94518	13.774 ± 0.05	3.872 ± 0.01	0.351 ± 0.003	0.85 ± 0.06	4.00 ± 0.005	3.86
HD 147609	4.301 ± 0.107	1.955 ± 0.055	1.118 ± 0.02	1.70 ± 0.05	3.71 ± 0.02	3.50
HD 154276	11.554 ± 0.025	4.339 ± 0.005	0.164 ± 0.002	1.00 ± 0.05	4.29 ± 0.002	4.28
HD 179832	2.914 ± 0.052	0.216 ± 0.041	1.814 ± 0.02	2.5 ± 0.28	2.70 ± 0.02	2.70
HD 207585	5.3146 ± 0.407	3.313 ± 0.165	0.575 ± 0.065	1.05 ± 0.05	3.90 ± 0.045	3.80
HD 211173	3.387 ± 0.066	0.839 ± 0.042	1.564 ± 0.02	2.20 ± 0.24	2.93 ± 0.02	2.60
HD 219116	1.584 ± 0.044	0.002 ± 0.06	1.901 ± 0.02	2.35 ± 0.17	2.68 ± 0.015	2.50

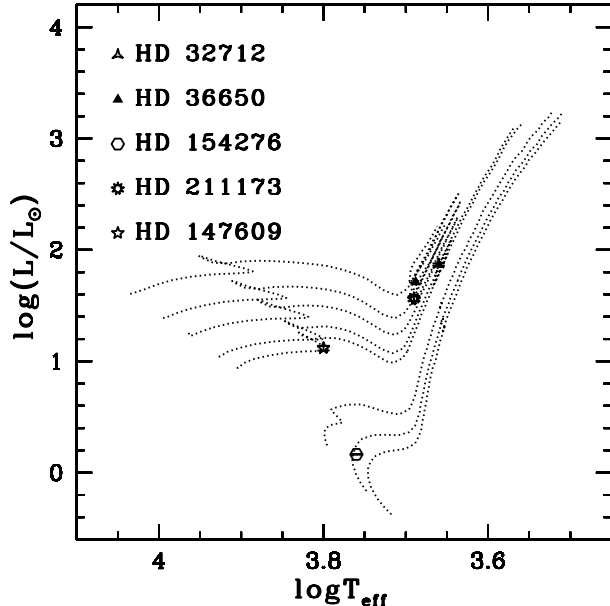


Figure 2. The locations of HD 32712, HD 36650, HD 154276, HD 211173 and HD 147609. The evolutionary tracks for 0.9, 1.0, 1.2, 1.7, 1.8, 2.0, 2.2, and 2.5 M_{\odot} are shown from bottom to top for $z = 0.019$.

to different elements are identified by comparing closely the spectra of program stars with the Doppler corrected spectrum of the star Arcturus. The $\log gf$ and the lower excitation potential values of the lines are taken from the Kurucz database of atomic line lists. The equivalent width of the spectral lines are measured using various tasks in IRAF. A master line list including all the elements was generated. For the elements showing hyper-fine splitting and for molecular bands, spectrum synthesis of MOOG was used to find the abundances. Elements Sc, V, Mn, Co, Cu, Ba, La and Eu are affected by Hyper-fine Splitting. The hyper-fine components of Sc and Mn are taken from Prochaska & McWilliam 2000, V, Co and Cu from Prochaska et al. 2000, Ba from McWilliam 1998, La from Jonsell et al. 2006, Eu from Worely et al. 2013. All the abundances are found relative to the respective solar values (Asplund et al. 2009).

The abundance estimates are given in Tables 6 through 8 and the lines used for the the abundance estimation are presented in Tables 11 and 12. The detailed abundance analyses and discussion are given in the section 6.

5 ABUNDANCE UNCERTAINTIES

The uncertainties in the elemental abundances has two main components: random error and systematic error. Random error arises from the uncertainties in the line parameters such as measured equivalent width, line blending and oscillator strength. Since the random error varies inversely as

Table 4. Comparison of estimated stellar parameters with literature values

Star	T_{eff} (K)	$\log g$	ζ (km s^{-1})	[Fe I/H]	[Fe II/H]	Ref.
HD 24035	4750	2.20	1.58	-0.51	-0.50	1
	4700	2.50	1.30	-0.23	-0.28	2
	4500	2.00	-	-0.14	-	3
HD 32712	4550	2.53	1.24	-0.25	-0.25	1
	4600	2.10	1.30	-0.24	-0.25	2
HD 36650	4880	2.40	1.30	-0.02	-0.02	1
	4800	2.30	1.50	-0.28	-0.28	2
HD 94518	5700	3.86	1.30	-0.55	-0.55	1
	5859	4.20	4.15	-0.56	-	4
	5859	4.15	1.20	-0.49	-0.50	5
	5709	3.86	2.23	-0.84	-	6
HD 147609	6350	3.50	1.55	-0.28	-0.28	1
	6411	3.90	1.26	-0.23	-	7
	5960	3.30	1.50	-0.45	+0.08	8
	6270	3.50	1.20	-	-	9
	6300	3.61	1.20	-	-	10
HD 154276	5820	4.28	0.63	-0.09	-0.10	1
	5722	4.28	0.93	-0.29	-	5
	5731	4.35	1.28	-0.30	-	11
HD 179832	4780	2.70	0.99	+0.23	+0.22	1
HD 207585	5800	3.80	1.00	-0.38	-0.38	1
	5800	4.00	-	-0.20	-	3
	5400	3.30	1.80	-0.57	-	12
	5400	3.50	1.50	-0.50	-	13
HD 211173	4900	2.60	1.15	-0.17	-0.17	1
	4800	2.50	-	-0.12	-	3
HD 219116	5050	2.50	1.59	-0.45	-0.44	1
	4900	2.30	1.60	-0.61	-0.62	2
	4800	1.80	-	-0.34	-	3
	5300	3.50	2.00	-0.30	-	14
	5300	3.50	-	-0.34	-	15

References: 1. Our work, 2. de Castro et al. (2016), 3. Masseron et al. (2010), 4. Battistini & Bensby (2015), 5. Bensby et al. (2014), 6. Axer et al. (1994), 7. Escorza et al. (2019) 8. Allen & Barbuy (2006a), 9. North et al. (1994a), 10. Thévenin & Idiart (1999), 11. Ramirez et al. (2013), 12. Luck & Bond (1991), 13. Smith & Lambert (1986a), 14. Smith et al. (1993), 15. Cenarro et al. (2007)

the square-root of the number of lines, we can reduce this error by using maximum possible number of lines. Systematic error is due to the uncertainties in the adopted stellar atmospheric parameters. The total uncertainty in the elemental abundance $\log \epsilon$ is calculated as;

$$\sigma_{\log \epsilon}^2 = \sigma_{ran}^2 + \left(\frac{\partial \log \epsilon}{\partial T}\right)^2 \sigma_{T_{eff}}^2 + \left(\frac{\partial \log \epsilon}{\partial \log g}\right)^2 \sigma_{\log g}^2 +$$

$$\left(\frac{\partial \log \epsilon}{\partial \zeta}\right)^2 \sigma_{\zeta}^2 + \left(\frac{\partial \log \epsilon}{\partial [\text{Fe}/\text{H}]}\right)^2 \sigma_{[\text{Fe}/\text{H}]}^2$$

where $\sigma_{ran} = \frac{\sigma_s}{\sqrt{N}}$. σ_s is the standard deviation of the abundances derived from the N number of lines of the particular species. The σ 's are the typical uncertainties in the stellar atmospheric parameters, which are $T_{eff} \sim \pm 100$ K, $\log g \sim \pm 0.2$ dex, $\zeta \sim \pm 0.2$ km s^{-1} and $[\text{Fe}/\text{H}] \sim \pm 0.1$ dex. The abundance uncertainties arising from the error of each stellar atmospheric parameters is estimated by varying one parameter at a time by an amount equal to their corresponding uncertainty, by keeping others the same and computing the changes in the abundances. We have done this procedure for a representative star, HD 211173, in our sample with the assumption that the uncertainties due to different parameters are independent, following de Castro et al. (2016), Karinkuzhi et al. (2018) and Cseh et al. (2018). The esti-

mated differential abundances is given in Table 5. The procedure has been applied to the abundances estimated from the equivalent width measurement as well as the spectral synthesis calculation. Finally, the uncertainty in $[\text{X}/\text{Fe}]$ is calculated as,

$$\sigma_{[\text{X}/\text{Fe}]}^2 = \sigma_X^2 + \sigma_{Fe}^2 .$$

6 ABUNDANCE ANALYSIS AND DISCUSSION

6.1 Light element abundance analysis: C, N, O, $^{12}\text{C}/^{13}\text{C}$, Na, Al, α - and Fe-peak elements

The [O I] line at 6300.304 Å is used to derive the oxygen abundances, whenever possible, otherwise, the resonance O I triplet lines at around 7770 Å are used. The O I triplet lines are known to be affected by the non-LTE effects (Eriksson & Toft 1979, Johnson et al. 1974, Baschek et al. 1977, Kiselman 1993, Amarsi et al. 2016). The corrections are made to the LTE abundance obtained with these lines following Bensby et al. (2004) and Afsar et al. (2012). The [O I] line at 6363.776 Å, is found to be blended and not usable for abundance determination in any of the stars. The spectrum synthesis fits of O I triplet lines for a few program stars are

Table 5. Differential Abundance ($\Delta\log\epsilon$) of different species due to the variations in stellar atmospheric parameters for HD 211173

Element	ΔT_{eff} (+100 K)	ΔT_{eff} (-100 K)	$\Delta\log g$ (+0.2 dex)	$\Delta\log g$ (-0.2 dex)	$\Delta\zeta$ (+0.2 kms ⁻¹)	$\Delta\zeta$ (-0.2 kms ⁻¹)	$\Delta[\text{Fe}/\text{H}]$ (+0.1 dex)	$\Delta[\text{Fe}/\text{H}]$ (-0.1 dex)	$(\Sigma\sigma_i^2)^{1/2}$ ($+\Delta$)	$(\Sigma\sigma_i^2)^{1/2}$ ($-\Delta$)	$\sigma_{[\text{X}/\text{Fe}]}$ ($+\Delta$)	$\sigma_{[\text{X}/\text{Fe}]}$ ($-\Delta$)
C	0.00	0.00	+0.03	-0.03	-0.03	+0.03	+0.01	-0.01	0.04	0.04	0.19	0.18
N	+0.10	-0.10	0.00	0.00	+0.02	-0.02	+0.05	-0.05	0.11	0.11	0.21	0.21
O	-0.19	+0.19	+0.06	-0.06	0.00	0.00	0.00	0.00	0.20	0.20	0.27	0.26
Na I	+0.07	-0.08	-0.02	+0.02	-0.05	+0.05	0.00	+0.01	0.09	0.10	0.21	0.21
Mg I	+0.06	-0.05	0.00	+0.01	-0.06	+0.07	0.00	+0.01	0.08	0.09	0.21	0.20
Al I	+0.06	-0.07	0.00	0.00	-0.02	+0.02	0.00	0.00	0.06	0.07	0.20	0.19
Si I	-0.03	+0.03	+0.04	-0.04	-0.03	+0.03	+0.01	-0.01	0.06	0.06	0.20	0.20
Ca I	+0.10	-0.11	-0.04	+0.03	-0.10	+0.09	0.00	0.00	0.15	0.15	0.24	0.23
Sc II	-0.02	+0.02	+0.09	-0.09	-0.09	+0.08	+0.02	-0.03	0.13	0.13	0.22	0.21
Ti I	+0.14	-0.15	-0.01	+0.01	-0.08	+0.08	0.00	0.00	0.16	0.17	0.24	0.24
Ti II	-0.02	0.00	+0.07	-0.08	-0.10	+0.09	+0.02	-0.03	0.13	0.12	0.23	0.22
V I	+0.16	-0.17	-0.01	0.00	-0.07	+0.07	-0.01	+0.01	0.18	0.18	0.25	0.25
Cr I	+0.13	-0.13	-0.02	+0.02	-0.13	+0.12	0.00	0.00	0.18	0.18	0.26	0.25
Cr II	-0.08	+0.07	+0.10	-0.09	-0.08	+0.09	+0.01	-0.02	0.15	0.15	0.25	0.24
Mn I	+0.09	-0.10	-0.02	+0.01	-0.16	+0.14	-0.01	0.00	0.18	0.17	0.26	0.24
Fe I	+0.07	-0.07	0.00	-0.01	-0.13	+0.12	+0.10	-0.10	0.18	0.17	-	-
Fe II	-0.09	+0.07	+0.10	-0.10	-0.10	+0.09	+0.10	-0.10	0.20	0.18	-	-
Co I	+0.07	-0.07	+0.02	-0.03	-0.06	+0.06	+0.01	-0.02	0.09	0.10	0.20	0.20
Ni I	+0.04	-0.03	+0.02	-0.02	-0.10	+0.10	+0.01	-0.01	0.11	0.11	0.21	0.20
Cu I	+0.09	-0.09	-0.01	0.00	-0.15	+0.12	+0.03	-0.02	0.18	0.15	0.25	0.23
Zn I	-0.05	+0.06	+0.07	-0.06	-0.08	+0.09	+0.02	-0.01	0.12	0.12	0.22	0.21
Rb I	+0.10	-0.10	0.00	0.00	-0.03	+0.03	0.00	0.00	0.10	0.10	0.21	0.20
Sr I	+0.15	-0.16	-0.03	+0.02	-0.22	+0.22	0.00	+0.01	0.27	0.27	0.32	0.32
Y I	+0.16	-0.17	-0.01	0.00	-0.02	+0.03	0.00	+0.01	0.16	0.17	0.24	0.24
Y II	-0.01	0.00	+0.08	-0.08	-0.14	+0.14	+0.02	-0.03	0.16	0.16	0.24	0.24
Zr I	+0.17	-0.19	-0.01	0.00	-0.03	+0.03	-0.01	0.00	0.17	0.19	0.25	0.26
Zr II	-0.03	+0.01	+0.09	-0.09	-0.09	+0.11	+0.02	-0.03	0.13	0.15	0.22	0.23
Ba II	+0.02	-0.03	+0.05	-0.06	-0.19	+0.15	+0.03	-0.04	0.20	0.17	0.27	0.24
La II	+0.01	0.00	+0.09	-0.09	-0.06	+0.07	+0.03	-0.03	0.11	0.12	0.21	0.21
Ce II	+0.01	-0.01	+0.09	-0.08	-0.11	+0.15	+0.04	-0.03	0.15	0.17	0.23	0.25
Pr II	+0.01	-0.02	+0.08	-0.09	-0.03	+0.03	+0.03	-0.04	0.09	0.10	0.22	0.21
Nd II	+0.01	-0.02	+0.08	-0.09	-0.09	+0.09	+0.03	-0.04	0.12	0.11	0.22	0.21
Sm II	+0.02	-0.02	+0.09	-0.08	-0.05	+0.07	+0.04	-0.03	0.11	0.11	0.21	0.21
Eu II	-0.02	+0.01	+0.09	-0.09	-0.03	+0.04	+0.03	-0.03	0.10	0.10	0.21	0.20

shown in Figure 3. All the three lines of the O I IR triplet gave the same abundance values, except for HD 147609. In the case of HD 147609, the lines at 7771 and 7774 Å, gave the same abundance and the line at 7775 Å, gave an abundance which is 0.15 dex lower. In this case, we have taken the average of the three values as the final oxygen abundance.

We have estimated the oxygen abundance in all the program stars except HD 24035. The derived abundance of oxygen is in the range $-0.26 \leq [\text{O}/\text{Fe}] \leq 0.97$. Oxygen is under abundant in HD 36650 and HD 211173 with $[\text{O}/\text{Fe}]$ values -0.23 and -0.26 respectively. HD 32712 and HD 179832 show near-solar values. Purandardas et al. (2019) found $[\text{O}/\text{Fe}] \sim -0.33$ for a barium star in their sample, somewhat closer to our lower limit. A mild overabundance is found in the stars HD 154276 and HD 219116 with $[\text{O}/\text{Fe}]$ values 0.38 and 0.21 respectively. In the other three stars, we found an $[\text{O}/\text{Fe}] > 0.6$, with HD 207585 showing the largest enhancement of 0.97. The first dredge-up (FDU) is not expected to alter the oxygen abundance.

The carbon abundances are derived using the spectral synthesis calculation of C₂ band at 5165 Å, (Figure 4) for six objects. G-band of CH at 4300 Å, is used for two stars as the C₂ band at 5165 Å, are not usable for the abundance determination. The objects for which we could estimate the carbon abundance using both C₂ and CH bands, we find that the CH band returns a lower value for carbon by about 0.2 to 0.3 dex. We could determine the carbon abundance in all the objects except for HD 154276 and HD 179832. Carbon is found to be under abundant in most of the stars analyzed here. The $[\text{C}/\text{Fe}]$ value ranges from -0.28 to 0.61. The stars HD 24035, HD 147609 and HD 207585 show a mild over abundance of carbon with values 0.41, 0.38 and

0.61 respectively, whereas it is near-solar in HD 32712 and HD 219116. HD 36650, HD 94518 and HD 211173 show mild under abundance with $[\text{C}/\text{Fe}]$ values, -0.22 , -0.28 , -0.23 respectively. These values are consistent with those generally noticed in barium stars (Barbuy et al. 1992, North et al. 1994a).

With the estimated carbon abundances, we have derived the abundances of nitrogen using the spectrum synthesis calculation of ¹²CN lines at 8000 Å region in HD 32712, HD 36650, HD 94518 and HD 211173. In other objects, where this region is not usable or unavailable, CN band at 4215 Å is used. The molecular lines for CN and C₂ are taken from Brooke et al. (2013), Sneden et al. (2014) and Ram et al. (2014).

The nitrogen abundance is estimated in seven of the program stars. Estimated $[\text{N}/\text{Fe}]$ values range from 0.24 to 1.41 dex with HD 24035 and HD 94518 showing $[\text{N}/\text{Fe}] > 1.0$ dex. Such higher values of nitrogen have already been noted in some barium stars by several authors (Smith 1984, Luck & Lambert 1985, Barbuy et al. 1992, Allen & Barbuy 2006a, Smiljanic et al. 2006, Merle et al. 2016, Karinkuzhi et al. 2018). Nitrogen enhancement with $[\text{N}/\text{Fe}] > 1$ is possible if the star is previously enriched by the pollution from a massive AGB companion experiencing Hot-Bottom Burning (HBB). In super-massive AGB stars nitrogen can be substantially produced at the base of the convective envelope when the temperature of the envelope exceeds 10⁸ K (Doherty et al. 2014a).

We could derive the carbon isotopic ratio, ¹²C/¹³C, using the spectral synthesis calculation of the ¹²CN lines at 8003.292, 8003.553, 8003.910 Å, and ¹³CN features at 8004.554, 8004.728, 8004.781 Å, for four stars, HD 32712,

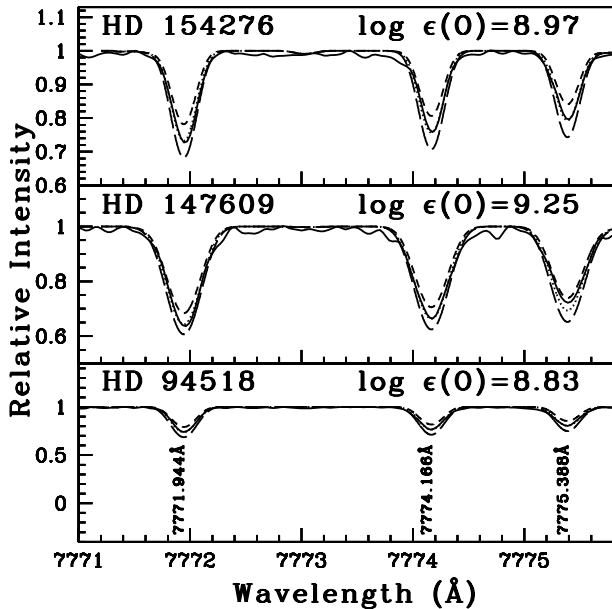
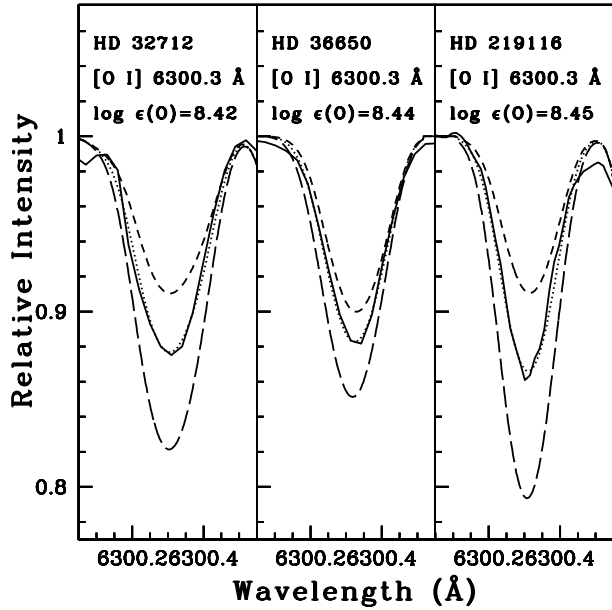


Figure 3. Synthesis of [O I] line around 6300 Å (Top panel) and O I triplet around 7770 Å (Bottom panel, LTE abundance estimates). Dotted line represents synthesized spectra and the solid line indicates the observed spectra. Short dashed line represents the synthetic spectra corresponding to $\Delta[\text{O}/\text{Fe}] = -0.3$ and long dashed line is corresponding to $\Delta[\text{O}/\text{Fe}] = +0.3$.

HD 36650, HD 211173 and HD 219116. The values for this ratio are 20.0, 7.34, 20.0 and 7.34 respectively. Values in the range 7 - 20 (Barbuy et al. 1992, Smith et al. 1993, Smith 1984, Harris et al. 1985, Karinkuzhi et al. 2018), and 13 -33 (Tomkin & Lambert 1979, Sneden et al. 1981) are found in literature for barium stars.

The lower level of carbon enrichment and low $^{12}\text{C}/^{13}\text{C}$ ratio along with larger over abundance of nitrogen indicate that the matter has undergone CN processing and the products have been brought to the surface by the FDU. From

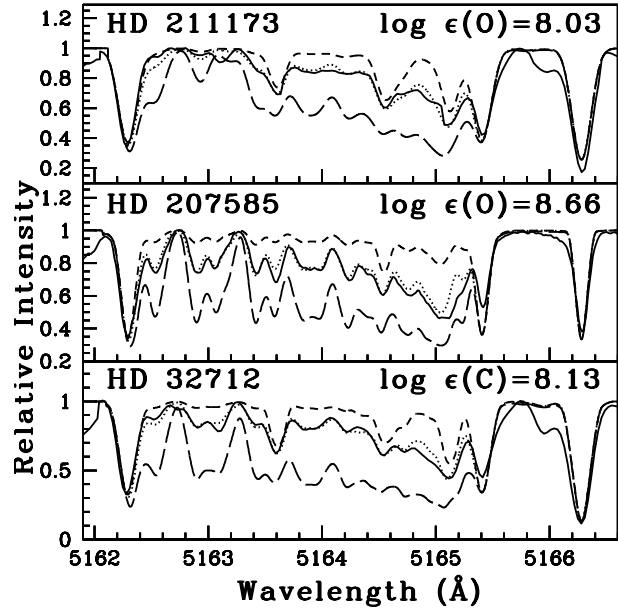


Figure 4. Synthesis of C_2 band around 5165 Å. Dotted line represents synthesized spectra and the solid line indicates the observed spectra. Short dashed line represents the synthetic spectra corresponding to $\Delta[\text{C}/\text{Fe}] = -0.3$ and long dashed line is corresponding to $\Delta[\text{C}/\text{Fe}] = +0.3$.

their locations in HR diagram, the three stars for which we could estimate $^{12}\text{C}/^{13}\text{C}$ ratio are on the ascent of first giant branch (FGB). These stars have undergone the FDU at the beginning of FGB. It has been noted that less evolved barium stars show higher carbon abundance as they have not reached the FDU (Barbuy et al. 1992, Allen & Barbuy 2006a). Among our program stars, HD 207585 shows the maximum enhancement of carbon, which is on the subgiant branch. However, the star HD 94518 shows the least enrichment among the program stars despite being the less evolved one, dwarf barium star. According to Vanture (1992), if the accreted material is mixed to the hydrogen burning region of the star either during the main-sequence or the first ascent of the giant branch, certain nucleosynthesis can happen, thereby reducing the carbon abundance. Smiljanic et al. (2006) ascribes rotational mixing for reduction in the surface carbon abundance. Also, even though the star has not reached the stage of dredge-up, the difference in the mean molecular weight of the accreted material and the inherent stellar materials in the interiors can induce thermohaline mixing, and this could reduce the surface carbon abundance by an order of magnitude compared to the unaltered case (Stancliffe et al. 2007).

We have estimated the C/O ratios of the program stars except for HD 24035, HD 154276 and HD 179832. The estimated $\text{C}/\text{O} < 1$ as normally seen in barium stars (Table 13).

The estimated Na abundances in the range $0.05 \leq [\text{Na}/\text{Fe}] \leq 0.42$ are similar to what is normally seen for disk stars, normal field giants and some barium stars (Antipova et al. 2004, de Castro et al. 2016, Karinkuzhi et al. 2018). Na, Mg and Al are produced in the carbon burning stages of massive stars (Woosely & Weaver 1995), hence the SN II are the probable sources of these elements in the disk.

The thick and thin disk dwarf stars in the Galaxy do not show any trend in $[\text{Na}/\text{Fe}]$ ratio with metallicity (Edvardsson et al. 1993, Reddy et al. 2003, Reddy et al. 2006). Similar pattern as the dwarf stars is observed in the case of field giants (Mishenina et al. 2006, Luck & Heiter 2007). Owing to the common origin, all the stars in the disk is expected to show similar abundance. An enhanced abundance of Na can be expected in AGB stars during the inter-pulse stage from ^{22}Ne produced in the previous hot pulses via $^{22}\text{Ne}(\text{p}, \gamma)^{23}\text{Na}$ (NeNa chain) (Mowlavi 1999, Goriely & Mowlavi 2000). This Na can be brought to the surface during TDU. Hence an overabundance of Na may be expected in the barium stars. However Na enrichment can be expected in stars prior to the AGB phase. El Eid & Champagne (1995) and Antipova et al. (2004) related this over abundance of Na to the nucleosynthesis associated with the evolutionary stage of the star. According to them, Na is synthesized in the convective H-burning core of the main-sequence stars through NeNa chain. Later, this products are mixed to the surface during the FDU. As a result, it is possible to observe sodium enrichment in giants rather than in dwarfs. Boyarchuk et al. (2001), de Castro et al. (2016) found an anti-correlation of $[\text{Na}/\text{Fe}]$ with $\log g$. We could observe a similar trend in our sample. According to Denissenkov & Ivanov (1987), a star with a minimum mass of $1.5M_{\odot}$ will be able to raise the Na abundance through the NeNa chain even in the main-sequence itself. Even though the Na enriched material can be synthesized in AGB and subsequently transferred to the barium stars, there may be a non-negligible contribution to the Na enrichment from the barium star itself.

The derived abundance of aluminium in HD 154276 and HD 211173 return near-solar values for $[\text{Al}/\text{Fe}]$, -0.12 and -0.11 respectively. Yang et al. (2016) found a range $-0.22 \leq [\text{Al}/\text{Fe}] \leq 0.56$, Allen & Barbuy (2006a) $-0.1 \leq [\text{Al}/\text{Fe}] \leq 0.1$, and de castro et al. (2016) $-0.07 \leq [\text{Al}/\text{Fe}] \leq 0.43$ for their sample of barium stars.

The estimated abundances of Mg are in the range $-0.10 \leq [\text{Mg}/\text{Fe}] \leq 0.44$. A Mg enrichment is expected to observe in the barium stars if the s-process over abundance is resulting from the neutrons produced during the convective thermal pulses through the reaction $^{22}\text{Ne}(\alpha, n)^{25}\text{Mg}$. We could not find any enhancement for Mg in our sample when compared with values from the disk stars and normal giants. This discards the fact that the origin of neutron is $^{22}\text{Ne}(\alpha, n)^{25}\text{Mg}$ source.

The estimated abundances for other elements, from Si, to Zn are found to be well-within the range as normally seen for disk stars.

6.2 Heavy element abundance analysis

6.2.1 The light s-process elements: Rb, Sr, Y, Zr

The abundance of Rb is derived using the spectral synthesis calculation of Rb I resonance line at 7800.259 \AA in the stars HD 32712, HD 36650, HD 179832 and HD 211173. We could not detect the Rb I lines in the warmer program stars. The Rb I resonance line at 7947.597 \AA is not usable for the abundance estimation. The hyperfine components of Rb is taken from Lambert & Luck (1976). The spectrum synthesis of Rb for the three program stars are shown in Figure

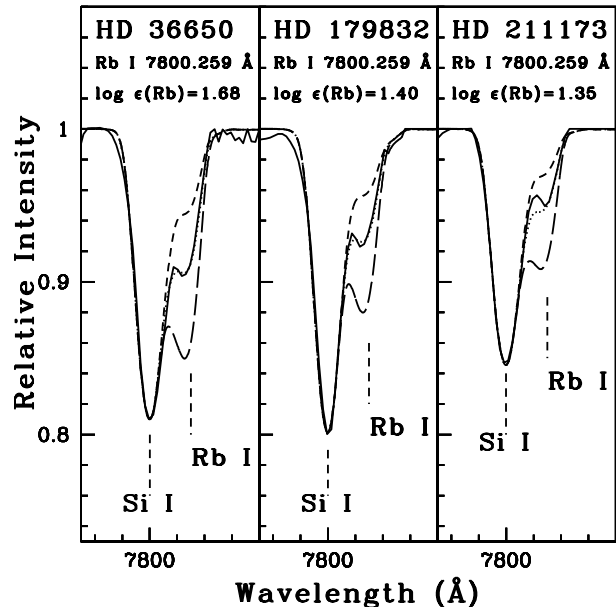


Figure 5. Synthesis of Rb I line around 7800 \AA . Dotted line represents synthesized spectra and the solid line indicates the observed spectra. Short dashed line represents the synthetic spectra corresponding to $\Delta[\text{Rb}/\text{Fe}] = -0.3$ and long dashed line is corresponding to $\Delta[\text{Rb}/\text{Fe}] = +0.3$

5. Rubidium is found to be under abundant in all the four program stars with $[\text{Rb}/\text{Fe}]$ ranging from -1.35 to -0.82 .

Strontium abundances are derived from the spectral synthesis calculation of Sr I line at 4607.327 \AA whenever possible. HD 154276 shows a mild under abundance with value $[\text{Sr}/\text{Fe}] \sim -0.22$, while HD 32712 and HD 179832 show near-solar values. Other stars show enrichment with value $[\text{Sr}/\text{Fe}] > 0.66$.

The abundance of Y is derived from the spectral synthesis calculation of Y I line at 6435.004 \AA in all the program stars except for HD 94518, HD 147609, HD 154276 and HD 179832 where no useful Y I line were detected. The spectral synthesis of Y II line at 5289.815 \AA is used in HD 94518 while the equivalent width measurement of several lines of Y II is used in other stars. The abundances estimated from Y I lines range from 0.38 to 1.61 , and that from Y II lines, 0.07 to 1.37 .

The spectral synthesis of Zr I line at 6134.585 \AA is used in all the stars except HD 94518, HD 147609 and HD 154276 where this line was not detected. We could detect useful Zr II lines in all the program stars except HD 36650 and HD 219116. In HD 24035, the equivalent width measurement of Zr II lines at 4317.321 and 5112.297 \AA are used. Spectral synthesis calculation of Zr II line at 4208.977 \AA is used in HD 94518, HD 147609 and HD 154276, line at 5112.297 \AA is used in HD 32712, HD 179832, HD 207585 and HD 211173. The measurement using Zr I lines gives the value $0.38 \leq [\text{Zr I}/\text{Fe}] \leq 1.29$ and Zr II lines return $-0.08 \leq [\text{Zr II}/\text{Fe}] \leq 1.89$. The spectrum synthesis of Zr for a few program stars are shown in Figure 6.

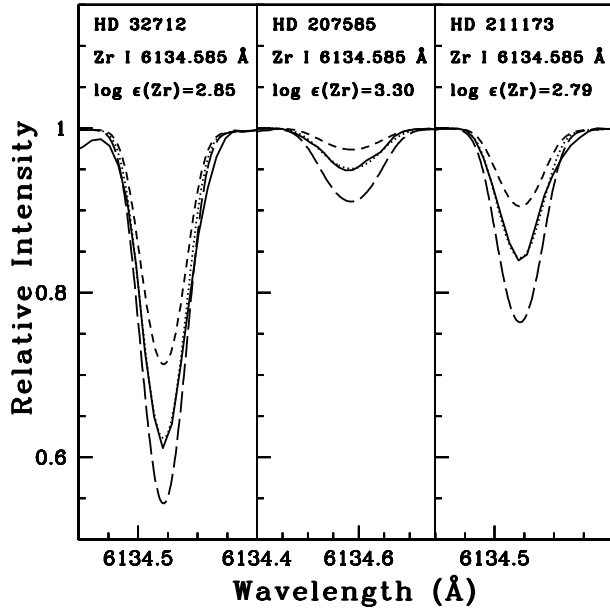


Figure 6. Synthesis of Zr I line at 6134.585 Å. Dotted line represents synthesized spectra and the solid line indicates the observed spectra. Short dashed line represents the synthetic spectra corresponding to $\Delta[\text{Zr}/\text{Fe}] = -0.3$ and long dashed line is corresponding to $\Delta[\text{Zr}/\text{Fe}] = +0.3$

6.2.2 The heavy s-process elements: Ba, La, Ce, Pr, Nd

The abundance of Ba is derived from the spectral synthesis. Ba II lines at 5853.668, 6141.713 and 6496.897 Å are used in HD 154276, whereas, in all the other stars, we have used the line at 5853.668 Å. The spectrum synthesis fits for Ba for a few program stars are shown in Figure 7. Ba shows slight overabundance in HD 154276 with $[\text{Ba}/\text{Fe}] \sim 0.22$, while HD 179832 and HD 211173 show moderate enhancement with values 0.41 and 0.57 respectively. All other program stars show the overabundance of Ba in the range 0.79 to 1.71.

Lanthanum abundance is obtained from the spectral synthesis analysis of La II line at 4322.503 Å in HD 147609. For all other stars spectral synthesis analysis of La II line at 4921.776 Å is used. The estimated La abundances are in the range $0.20 \leq [\text{La}/\text{Fe}] \leq 1.70$. HD 154276 shows a mild enhancement of La with $[\text{La}/\text{Fe}] \sim 0.20$. All other program stars are overabundant in La with $[\text{La}/\text{Fe}]$ ranging from 0.52 to 1.70.

The abundances of Ce is obtained from the equivalent width measurement of several The star HD 154276 show near-solar abundance for Ce with $[\text{Ce}/\text{Fe}] \sim 0.18$, whereas all other stars are overabundant in Ce with $[\text{Ce}/\text{Fe}] > 0.7$.

The abundance of Pr is derived from the the equivalent width measurement of Pr II lines whenever possible. We could not estimate Pr abundance in HD 94518 and HD 154276 as there were no useful lines detected. HD 179832 is mildly enhanced in Pr with $[\text{Pr}/\text{Fe}] \sim 0.23$ while other stars show the enrichment in the range 0.85 to 1.98.

Abundance of Nd is estimated from the spectral synthesis calculation of Nd II lines at 4177.320 and 4706.543 Å in

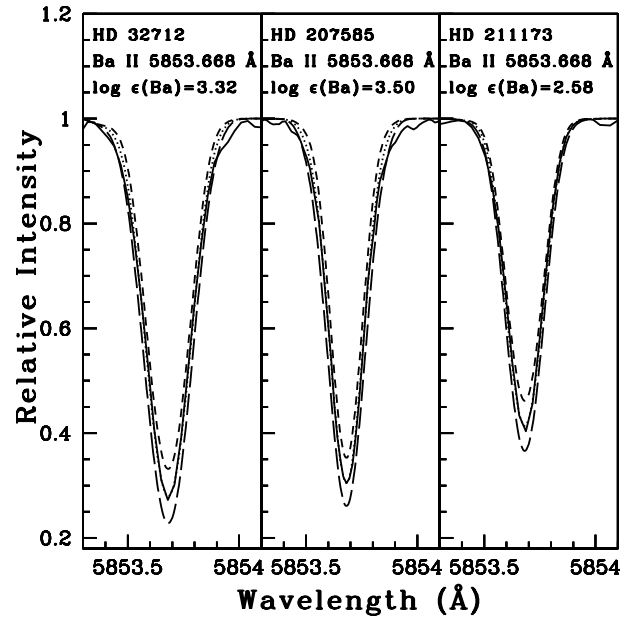


Figure 7. Synthesis of Ba II line at 5853.668 Å. Dotted line represents synthesized spectra and the solid line indicates the observed spectra. Short dashed line represents the synthetic spectra corresponding to $\Delta[\text{Ba}/\text{Fe}] = -0.3$ and long dashed line is corresponding to $\Delta[\text{Ba}/\text{Fe}] = +0.3$

HD 154276. In all other stars, we have used the equivalent width measurement of several Nd II lines. A near-solar value is obtained for the Nd abundance in the star HD 179832 with $[\text{Nd}/\text{Fe}] \sim 0.04$, whereas a moderate enhancement is found in HD 154276 with $[\text{Nd}/\text{Fe}] \sim 0.40$. All other objects show an enrichment in Nd with $[\text{Nd}/\text{Fe}] > 0.81$.

6.3 The r-process elements: Sm, Eu

Samarium abundance is derived by the spectral synthesis of Sm II line at 4467.341 Å in HD 154276. The equivalent width measurement of several Sm II lines is used to obtain the Sm abundance in the rest of the program stars. All the good Sm lines are found in the bluer wavelength region of the spectra. The maximum number of Sm II lines used is eight, in HD 207585. The estimated Sm abundances give a near-solar value for HD 154276 with $[\text{Sm}/\text{Fe}] \sim 0.07$ while all other stars are enriched in Sm with values ranging from 0.78 to 2.04.

The Eu abundance is derived from the spectral synthesis of Eu II line at 4129.725 Å in HD 94518, HD 147609 and HD 207585. In all other stars except HD 154276, spectral synthesis calculation of Eu II line at 6645.064 Å is used. In HD 154276, no useful lines for abundance analysis is detected. The estimated Eu abundance covers the range $0.00 \leq [\text{Eu}/\text{Fe}] \leq 0.49$. The r-process element Eu is not expected to show enhancement in Ba stars according to their formation scenario.

The observed abundance ratios when compared with their counterparts in other barium stars from literature, the light as well as the heavy element Eu are found to follow the Galactic trend.

In order to find the s-process contents in the stars, we

have estimated the mean abundance ratio of the s-process elements (Sr, Y, Zr, Ba, La, Ce, Nd), $[\text{s}/\text{Fe}]$, for our stars. The estimated values of $[\text{s}/\text{Fe}]$ is provided in Table 13. The star HD 154276 shows the least value for $[\text{s}/\text{Fe}]$ ratio. A comparison of $[\text{s}/\text{Fe}]$ ratio observed in our program stars with that in Ba stars and normal giants from literature is shown in Figure 8. The stars which are rejected as Ba stars from the analysis of de Castro et al. (2016) are also shown for a comparison. The $[\text{s}/\text{Fe}]$ value of HD 154276 falls among these rejected stars. Most of these rejected Ba stars are listed as marginal Ba stars in MacConnell et al. (1972). There is no clear mention in literature on how high should be the $[\text{s}/\text{Fe}]$ value for a star to be considered as a Ba star. According to de Castro et al. (2018), this value is +0.25, while Sneden et al. (1981) found a value +0.21, Pilachowski (1977) found +0.50 and Rojas et al. (2013) found a value >0.34 . If we stick on to the values of these authors, the star HD 154276 with $[\text{s}/\text{Fe}] = 0.11$, can not be consider as a Ba star. However, if we follow the criteria of Yang et al. (2016) that $[\text{Ba}/\text{Fe}]$ should be atleast 0.17 for the star even to be a mild star, HD 154276 can be considered as a mild Ba star with $[\text{Ba}/\text{Fe}] \sim 0.22$.

A comparison of the heavy element abundances with the literature values whenever available are presented in Table 10. In most of the cases our estimates agree within error bars with the literature values.

6.4 The $[\text{hs}/\text{ls}]$ ratio as an indicator of neutron source

In Table 13, we have presented the estimated $[\text{ls}/\text{Fe}]$, $[\text{hs}/\text{Fe}]$ and $[\text{hs}/\text{ls}]$ ratios for the program stars, where ls refers to the light s-process elements (Sr, Y and Zr) and hs to the heavy s-process elements (Ba, La, Ce and Nd).

The $[\text{hs}/\text{ls}]$ ratio is a useful indicator of neutron source in the former AGB star. As the metallicity decreases, the neutron exposure increases. As a result, lighter s-process elements are bypassed in favour of heavy elements. Hence, $[\text{hs}/\text{ls}]$ ratio increases with decreasing metallicity. The models of Busso et al. (2001) have shown the behaviour of this ratio with metallicity for AGB stars of mass 1.5 and 3.0 M_{\odot} for different ^{13}C pocket efficiencies. According to these models, the maximum value of $[\text{hs}/\text{ls}]$ is ~ 1.2 which is at metallicities ~ -1.0 and ~ -0.8 for the 3 and 1.5 M_{\odot} models respectively for the standard ^{13}C pocket efficiency. In their models, Goriely & Mowlavi (2000), have shown the run of $[\text{hs}/\text{ls}]$ ratio with metallicity for different thermal pulses for AGB stars in the range 1.5-3 M_{\odot} . The maximum value of $[\text{hs}/\text{ls}] \sim 0.6$ occurs at metallicity ~ -0.5 . It was noted that, in all these models, the $[\text{hs}/\text{ls}]$ ratio does not follow a linear anti-correlation with metallicity, rather exhibits a loop like behaviour. The ratio increases with decreasing metallicity upto a particular value of $[\text{Fe}/\text{H}]$ and then starts to drop. Our $[\text{hs}/\text{ls}]$ ratio has a maximum value of ~ 1.15 which occurs at a metallicity of ~ -0.25 . The anti-correlation of $[\text{hs}/\text{ls}]$ suggest the operation of $^{13}\text{C}(\alpha, n)^{16}\text{O}$ neutron source, since $^{13}\text{C}(\alpha, n)^{16}\text{O}$ is found to be anti-correlated with metallicity (Clayton 1988, Wallerstein 1997).

As seen from the Table 13, all the stars show positive values for $[\text{hs}/\text{ls}]$ ratio. At metallicities higher than solar, a negative value is expected for this ratio and at lower metallicities, a positive value is expected for low-mass AGB stars where $^{13}\text{C}(\alpha, n)^{16}\text{O}$ is the neutron source (Busso et al. 2001,

Goriely & Mowlavi 2000). However, it is possible that AGB stars with masses in the range 5-8 M_{\odot} can also exhibit low $[\text{hs}/\text{ls}]$ ratios considering the $^{22}\text{Ne}(\alpha, n)^{25}\text{Mg}$ neutron source (Karakas & Lattanzio 2014). The models of Karakas & Lattanzio (2014) predicted that the ls elements are predominantly produced over the hs elements for AGB stars of mass 5 and 6 M_{\odot} . The $[\text{hs}/\text{ls}]$ ratio is correlated to the neutron exposure. The $^{22}\text{Ne}(\alpha, n)^{25}\text{Mg}$ source has smaller neutron exposure compared to the $^{13}\text{C}(\alpha, n)^{16}\text{O}$ source. Hence, in the stars where $^{22}\text{Ne}(\alpha, n)^{25}\text{Mg}$ operates, we expect a lower $[\text{hs}/\text{ls}]$ ratio. The lower neutron exposure of the neutrons produced from the ^{22}Ne source together with the predictions of low $[\text{hs}/\text{ls}]$ ratio in massive AGB star models have been taken as the evidence of operation of $^{22}\text{Ne}(\alpha, n)^{25}\text{Mg}$ in massive AGB stars. A Mg enrichment is expected in the stars where this reaction takes place. As none of our stars shows such an enrichment, we discard the possibility of $^{22}\text{Ne}(\alpha, n)^{25}\text{Mg}$ reaction as a possible neutron source for any of our program stars, with respect to $[\text{hs}/\text{ls}]$ ratio. This is also supported by our estimates of Rb and Zr as discussed in the following section.

6.5 Rb as a probe to the neutron density at the s-process site

In addition to the $[\text{hs}/\text{ls}]$ ratio, the abundance of rubidium can also provide clues to the mass of the companion AGB stars. The AGB star models predict higher Rb abundances for massive AGB stars where the neutron source is $^{22}\text{Ne}(\alpha, n)^{25}\text{Mg}$ reaction (Abia et al. 2001, van Raai et al. 2012). In the s-process nucleosynthesis path, the branching points at the unstable nuclei ^{85}Kr and ^{86}Rb controls the Rb production. The amount of Rb produced along this s-process path is determined by the probability of these unstable nuclei to capture the neutron before β -decaying, which in turn depends on the neutron density at the s-process site (Beer & Macklin 1989, Tomkin & Lambert 1983, Lambert et al. 1995).

The production of ^{87}Rb from ^{85}Kr and ^{86}Rb is possible only at higher neutron densities, $N_n > 5 \times 10^8 \text{ n/cm}^3$, Sr, Y, Zr etc. are produced otherwise (Beer 1991, Lugaro & Chieffi 2011). The ^{87}Rb isotope has magic number of neutrons and hence it is fairly stable against neutron capture. Also, the neutron capture cross-section of ^{87}Rb is very small ($\sigma \sim 15.7 \text{ mbarn}$ at 30 KeV) compared to that of ^{85}Rb ($\sigma \sim 234 \text{ mbarn}$) (Heil et al. 2008a). Hence, once the nucleus ^{87}Rb is produced, it will be accumulated. Therefore, the isotopic ratio $^{87}\text{Rb}/^{85}\text{Rb}$ could be a direct indicator of the neutron density at the s-process site, as a consequence help to infer the mass of the AGB star. But, it is impossible to distinguish the lines due to these two isotopes of Rb in the stellar spectra (Lambert & Luck 1976, García-Hernández et al. 2006). However, the abundance of Rb relative to other elements in this region of the s-process path, such as Sr, Y, and Zr, can be used to estimate the average neutron density of the s-process. Detailed nucleosynthesis models for the stars with masses between 5 - 9 M_{\odot} at solar metallicity predict $[\text{Rb}/(\text{Sr}, \text{Zr})] > 0$ (Karakas et al. 2012). A positive value of $[\text{Rb}/\text{Sr}]$ or $[\text{Rb}/\text{Zr}]$ ratio indicates a higher neutron density, whereas a negative value indicates a low neutron density. This fact has been used as evidence to conclude that $^{13}\text{C}(\alpha, n)^{16}\text{O}$ reaction act as the neutron source in M, MS and S

Table 6. Elemental abundances in HD 24035, HD 32712 and HD 36650

	HD 24035					HD 32712			HD 36650		
	Z	solar log ϵ *	log ϵ	[X/H]	[X/Fe]	log ϵ	[X/H]	[X/Fe]	log ϵ	[X/H]	[X/Fe]
C	6	8.43	8.33(syn)	-0.10	0.41	8.13(syn)	-0.3	-0.05	8.19(syn)	-0.24	-0.22
N	7	7.83	8.73(syn)	0.90	1.41	8.10(syn)	0.27	0.52	8.38(syn)	0.55	0.57
O	8	8.69	-	-	-	8.42(syn)	-0.27	-0.02	8.20(syn)	-0.49	-0.47
Na I	11	6.24	6.15±0.17(4)	-0.09	0.42	6.20±0.13(4)	-0.04	0.21	6.33±0.08(4)	0.09	0.11
Mg I	12	7.60	7.23(1)	-0.37	0.14	7.25±0.20(2)	-0.35	-0.10	7.69±0.04(2)	0.09	0.11
Si I	14	7.51	7.26±0.04(2)	-0.25	0.14	7.60±0.19(3)	0.09	0.34	7.28±0.10(3)	-0.23	-0.21
Ca I	20	6.34	5.91±0.13(10)	0.43	0.08	5.92±0.09(11)	-0.42	-0.17	6.23±0.12(16)	-0.11	-0.09
Sc II	21	3.15	2.65(syn)	-0.50	0.01	2.95(syn)	-0.20	0.05	3.08(syn)	-0.12	-0.10
Ti I	22	4.95	4.76±0.11(19)	-0.19	0.32	4.68±0.11(27)	-0.27	-0.02	4.92±0.09(24)	-0.03	-0.01
Ti II	22	4.95	4.68±0.03(2)	-0.27	0.24	4.75±0.11(5)	-0.20	0.05	4.97±0.14(7)	0.02	0.04
V I	23	3.93	3.30(syn)	-0.63	-0.12	3.46(syn)	-0.47	-0.22	3.92(syn)	-0.53	-0.51
Cr I	24	5.64	5.11±0.06(6)	-0.53	-0.02	5.33±0.17(7)	-0.31	-0.06	5.60±0.15(9)	-0.04	-0.02
Cr II	24	5.64	-	-	-	5.72±0.17(4)	0.08	0.33	5.54±0.08(3)	-0.10	-0.08
Mn I	25	5.43	4.85(syn)	-0.58	-0.07	4.86(syn)	-0.57	-0.32	5.08(syn)	-0.40	-0.38
Fe I	26	7.50	6.99±0.19(87)	-0.51	-	7.25±0.12(84)	-0.25	-	7.48±0.12(92)	-0.02	-
Fe II	26	7.50	7.00±0.16(7)	-0.50	-	7.25±0.15(9)	-0.25	-	7.48±0.14(6)	-0.02	-
Co I	27	4.99	4.67(syn)	-0.32	0.19	4.43(syn)	-0.56	-0.31	4.86(syn)	-0.43	-0.41
Ni I	28	6.22	6.07±0.14(13)	-0.15	0.36	6.04±0.18(11)	-0.18	0.07	6.33±0.10(11)	0.11	0.13
Cu I	29	4.19	-	-	-	-	-	-	4.57(syn)	-0.09	-0.07
Zn I	30	4.56	3.92(1)	-0.64	-0.13	4.42(1)	-0.14	0.11	-	-	-
Rb I	37	2.52	-	-	-	1.14(syn)	-1.38	-1.13	1.68(syn)	-0.84	-0.82
Sr I	38	2.87	-	-	-	2.65(syn)	-0.22	0.03	3.78(syn)	0.64	0.66
Y I	39	2.21	3.31(syn)	1.1	1.61	2.52(syn)	0.31	0.56	2.70(syn)	0.49	0.51
Y II	39	2.21	-	-	-	3.00±0.15(6)	0.79	1.04	2.89±0.13(10)	0.68	0.70
Zr I	40	2.58	3.28(syn)	0.7	1.21	2.85(syn)	0.27	0.52	3.07(syn)	0.49	0.51
Zr II	40	2.58	3.96±0.07(2)	1.38	1.89	3.15(syn)	0.57	0.82	-	-	-
Ba II	56	2.18	3.38(syn)	1.20	1.71	3.32(syn)	1.14	1.39	2.95(syn)	0.77	0.79
La II	57	1.10	2.22(syn)	1.12	1.63	2.10(syn)	1.00	1.25	1.81(syn)	0.60	0.62
Ce II	58	1.58	2.77±0.12(9)	1.19	1.70	3.01±0.11(11)	1.43	1.68	2.55±0.13(11)	0.97	0.99
Pr II	59	0.72	2.19±0.18(6)	1.47	1.98	2.14±0.18(6)	1.42	1.67	1.55±0.13(3)	0.83	0.85
Nd II	60	1.42	2.32±0.17(15)	0.90	1.41	2.93±0.18(11)	1.51	1.76	2.34±0.16(15)	0.92	0.94
Sm II	62	0.96	2.48±0.13(4)	1.52	2.03	2.42±0.17(6)	1.46	1.71	1.93±0.12(6)	0.97	0.99
Eu II	63	0.52	0.50(syn)	-0.02	0.49	0.61(syn)	0.09	0.34	0.59(syn)	0.07	0.09

* Asplund (2009), The number inside the paranthesis shows the number of lines used for the abundance determination.

stars (Lambert et al. 1995) and C stars must be low-mass AGB stars with $M < 3M_{\odot}$ (Abia et al. 2001). The observed [Rb/Zr] ratios in the AGB stars both in our Galaxy and the Magellanic Clouds show a value < 0 for low-mass AGB stars and a value > 0 for intermediate-mass (4-6 M_{\odot}) AGB stars (Plez et al. 1993, Lambert et al. 1995, Abia et al. 2001, García-Hernández et al. 2006, 2007, 2009, van Raai et al. 2012).

The estimated [Rb/Zr] and [Rb/Sr] ratios (Table 13) give negative values for our stars for which we could estimate these ratios. The observed [Rb/Fe] and [Zr/Fe] ratios are shown in Figure 9. The observed ranges of Rb and Zr in low- and intermediate-mass AGB stars (shaded regions) in the Galaxy and Magellanic Clouds are also shown for a comparison. It is clear that the abundances of Rb and Zr are consistent with the range normally observed in the low-mass AGB stars.

6.6 Comparison with FRUITY models and a parametric model based analysis

A publicly available (<http://fruity.iaa-teramo.inaf.it/>, Web sites of the Teramo Observatory (INAF)) data set for the s-process in AGB stars is the FRANEC Repository of Updated Isotopic Tables & Yields (FRUITY) models (Cristallo et al. 2009, 2011, 2015b). These models cover the whole range of metallicity observed for Ba stars from $z = 0.001$

to $z = 0.020$ for the mass range 1.3 - 6.0 M_{\odot} . The computations comprise of the evolutionary models starting from the pre-main sequence to the tip of AGB phase through the core He-flash. During the core H-burning, no core overshoot has been considered, a semi-convection is assumed during the core He-burning. The only mixing considered in this model is arising from the convection, additional mixing phenomena such as rotation is not considered here. The calculations are based on a full nuclear network considering all the stable and relevant unstable isotopes from hydrogen to bismuth. This includes 700 isotopes and about 1000 nuclear processes such as charged particle reactions, neutron captures, and β -decays (Straniero et al. 2006, Görres et al. 2000, Jaeger et al. 2001, Abbondanno et al. 2004, Patronis et al. 2004, Heil et al. 2008b). The details of the input physics and the computational algorithms are provided in Straniero et al. (2006). In this model, ^{13}C pocket is formed through time-dependent overshoot mechanisms, which is controlled by a free overshoot parameter (β) in the exponentially declining convective velocity function. This parameter is set in such a way that the neutrons released are enough to maximise the production of s-process elements. For the low-mass AGB star models (initial mass $< 4 M_{\odot}$), neutrons are released by the $^{13}\text{C}(\alpha, n)^{16}\text{O}$ reaction during the interpulse phase in radiative conditions, when temperatures within the pockets reaches $T \sim 1.0 \times 10^8$ K, with typical densities of $10^6 - 10^7$ neutrons cm^{-3} . However, in the case of the metal-rich mod-

Table 7. Elemental abundances in HD 94518, HD 147609 and HD 154276

	HD 94518				HD 147609				HD 154276			
	Z	solar log ϵ^*	log ϵ	[X/H]	[X/Fe]	log ϵ	[X/H]	[X/Fe]	log ϵ	[X/H]	[X/Fe]	
C	6	8.43	7.60(syn)	-0.83	-0.28	8.53(syn)	0.10	0.38	-	-	-	
N	7	7.83	8.63(syn)	0.80	1.35	-	-	-	-	-	-	
O	8	8.69	8.79(syn)	0.10	0.65	9.05(syn)	0.36	0.64	8.91(syn)	0.22	0.32	
Na I	11	6.24	5.88±0.06(4)	-0.44	0.11	6.26±0.19(2)	0.02	0.30	6.20±0.05(3)	-0.04	0.06	
Mg I	12	7.60	7.37±0.12(4)	-0.23	0.32	7.49±0.08(4)	-0.11	0.17	7.81±0.06(3)	0.21	0.31	
Al I	13	6.45	-	-	-	-	-	-	6.23±0.08(2)	-0.22	-0.12	
Si I	14	7.51	6.90±0.20(4)	-0.61	-0.06	7.37±0.05(4)	-0.14	0.14	7.54±0.05(5)	0.03	0.13	
Ca I	20	6.34	6.01±0.13(18)	-0.33	0.22	6.04±0.21(21)	-0.30	0.21	6.22±0.20(27)	-0.12	-0.02	
Sc II	21	3.15	2.72(syn)	-0.63	-0.08	2.90(syn)	-0.25	0.03	3.25(syn)	0.10	0.20	
Ti I	22	4.95	4.64±0.13(12)	-0.31	0.24	4.66±0.06(10)	-0.29	-0.01	5.02±0.17(27)	0.07	0.17	
Ti II	22	4.95	4.81±0.14(13)	-0.14	0.41	4.67±0.16(8)	-0.28	0.00	5.06±0.21(18)	0.11	0.21	
V I	23	3.93	3.15(syn)	-0.78	-0.23	3.53(syn)	-0.40	-0.12	3.90(syn)	-0.03	0.07	
Cr I	24	5.64	5.07±0.14(15)	-0.57	-0.02	5.29±0.15(9)	-0.35	-0.07	5.51±0.20(11)	-0.13	-0.03	
Cr II	24	5.64	5.06±0.19(4)	-0.58	-0.03	5.29±0.11(3)	-0.35	-0.07	5.53±0.07(5)	-0.11	-0.01	
Mn I	25	5.43	4.61(syn)	-1.1	-0.55	5.03(syn)	-0.40	-0.12	5.17±0.15(6)	-0.26	-0.16	
Fe I	26	7.50	6.95±0.10(110)	-0.55	-	7.22±0.16(151)	-0.28	-	7.41±0.13(150)	-0.09	-	
Fe II	26	7.50	6.95±0.12(15)	-0.55	-	7.22±0.12(20)	-0.28	-	7.40±0.14(15)	-0.10	-	
Co I	27	4.99	4.52(syn)	-0.64	-0.09	-	-	-	4.85±0.10(2)	-0.14	-0.04	
Ni I	28	6.22	5.70±0.15(26)	-0.52	0.03	5.88±0.11(14)	-0.34	-0.06	6.13±0.15(19)	-0.09	0.01	
Cu I	29	4.19	3.67(syn)	-0.82	-0.27	-	-	-	-	-	-	
Zn I	30	4.56	4.15±0.10(2)	-0.41	0.14	4.30 ±0.07(2)	-0.26	0.02	4.64±0.00(2)	0.08	0.18	
Sr I	38	2.87	3.59(syn)	0.63	1.18	4.10(syn)	1.23	1.51	2.55(syn)	-0.32	-0.22	
Y II	39	2.21	2.16(syn)	-0.05	0.50	3.00±0.14(9)	0.79	1.07	2.18±0.19(4)	-0.03	0.07	
Zr II	40	2.58	2.32(syn)	-0.26	0.29	3.30(syn)	0.72	1.00	2.40(syn)	-0.18	-0.08	
Ba II	56	2.18	2.58(syn)	0.35	0.90	3.30(syn)	1.12	1.40	2.30(syn)	0.12	0.22	
La II	57	1.10	2.12(syn)	0.08	0.58	2.09(syn)	0.99	1.27	1.20(syn)	0.10	0.20	
Ce II	58	1.58	1.94±0.09(9)	0.36	0.91	2.56±0.11(8)	0.98	1.26	1.66±0.03(2)	0.08	0.18	
Pr II	59	0.72	-	-	-	1.79(1)	1.07	1.35	-	-	-	
Nd II	60	1.42	1.92±0.20(9)	0.50	1.05	2.21±0.17(8)	0.79	1.07	1.72±0.12(syn)(2)	0.30	0.40	
Sm II	62	0.96	1.80±0.08(4)	0.84	1.39	1.97±0.19(4)	1.01	1.29	0.93(syn)	-0.03	0.07	
Eu II	63	0.52	0.12(syn)	-0.40	0.15	0.37(syn)	-0.15	0.13	-	-	-	

* Asplund (2009), The number inside the parenthesis shows the number of lines used for the abundance determination.

Table 8. Elemental abundances in HD 179832, HD 207585, HD 211173 and HD 219116

	HD 179832				HD 207585				HD 211173				HD 219116			
	Z	solar log ϵ^*	log ϵ	[X/H]	[X/Fe]	log ϵ	[X/H]	[X/Fe]	log ϵ	[X/H]	[X/Fe]	log ϵ	[X/H]	[X/Fe]		
C	6	8.43	-	-	-	8.66(syn)	0.23	0.61	8.03(syn)	-0.40	-0.23	8.03(syn)	-0.43	0.02		
N	7	7.83	-	-	-	8.20(syn)	0.37	0.75	8.20(syn)	0.37	0.54	7.85(syn)	0.02	0.47		
O I	8	8.69	8.93(syn)	0.24	0.01	9.28(syn)	0.59	0.97	8.26(syn)	-0.43	-0.26	8.45(syn)	-0.24	0.21		
Na I	11	6.24	6.52±0.13(2)	0.28	0.05	6.11±0.11(4)	-0.13	0.25	6.30±0.14(4)	0.06	0.23	6.05±0.16(4)	-0.19	0.26		
Mg I	12	7.60	7.83±0.02(2)	0.23	0.00	7.29±0.12(3)	-0.31	0.07	7.66±0.08(2)	0.06	0.23	7.47±0.02(3)	-0.11	0.34		
Al I	13	6.45	-	-	-	-	-	-	6.17±0.07(2)	-0.28	-0.11	-	-	-		
Si I	14	7.51	7.71±0.08(4)	0.20	-0.03	7.25±0.02(2)	-0.26	0.12	6.97±0.11(2)	-0.54	-0.37	7.08±0.20(2)	-0.43	0.02		
Ca I	20	6.34	6.27±0.06(9)	-0.07	-0.30	6.22±0.17(11)	-0.12	0.26	6.23±0.17(15)	-0.11	0.06	6.02±0.14(16)	-0.34	0.13		
Sc II	21	3.15	3.35(syn)	0.20	-0.03	2.63(syn)	-0.52	-0.14	2.79(syn)	-0.36	-0.19	2.66(syn)	-0.49	-0.04		
Ti I	22	4.95	5.06±0.07(4)	0.11	-0.12	4.58±0.15(7)	-0.37	0.01	4.77±0.11(27)	-0.18	-0.01	4.73±0.09(21)	-0.22	0.23		
Ti II	22	4.95	5.39±0.08(4)	0.44	0.21	4.82±0.12(9)	-0.13	0.25	4.76±0.16(9)	-0.19	-0.02	4.65±0.15(6)	-0.3	0.15		
V I	23	3.93	4.03(syn)	0.10	-0.13	3.11(syn)	-0.82	-0.44	3.47(syn)	-0.46	-0.29	3.67(syn)	-0.26	0.19		
Cr I	24	5.64	5.78±0.12(2)	0.14	-0.09	5.39±0.15(11)	-0.25	0.13	5.45±0.16(11)	-0.19	-0.02	5.34±0.16(9)	-0.3	0.15		
Cr II	24	5.64	5.71±0.02(2)	0.07	-0.16	5.38±0.15(4)	-0.26	0.12	5.24±0.16(4)	-0.4	-0.23	5.20±0.09(2)	-0.44	0.01		
Mn I	25	5.43	5.25±0.09(3)	-0.18	-0.41	4.60(syn)	-0.83	-0.45	5.13(syn)	-0.30	-0.13	4.78(syn)	-0.65	0.2		
Fe I	26	7.50	7.73±0.01(68)	0.23	-	7.12±0.12(107)	-0.38	-	7.33±0.10(109)	-0.17	-	7.05±0.11(92)	-0.45	-		
Fe II	26	7.50	7.72±0.04(9)	0.22	-	7.12±0.11(12)	-0.38	-	7.33±0.09(11)	-0.17	-	7.06±0.12(9)	-0.44	-		
Co I	27	4.99	5.24±0.08(6)	0.25	0.02	4.55(syn)	-0.44	-0.06	4.58(syn)	-0.41	-0.24	4.69±0.10(7)	-0.3	0.15		
Ni I	28	6.22	6.43±0.07(10)	0.21	-0.02	5.83±0.14(16)	-0.39	-0.01	6.14±0.17(27)	-0.08	0.09	5.91±0.12(11)	-0.31	0.14		
Cu I	29	4.19	-	-	-	4.36(syn)	-0.63	-0.25	3.92(syn)	-0.27	-0.10	4.09(syn)	-0.12	0.33		
Zn I	30	4.56	4.94±0.11(2)	0.38	0.15	-	-	-	4.43±0.02(2)	-0.13	0.04	4.04(1)	-0.56	0.11		
Rb I	37	2.52	1.40(syn)	-1.12	-1.35	-	-	-	1.35(syn)	-1.17	-1.00	-	-	-		
Sr I	38	2.87	3.12(syn)	0.25	0.02	-	-	-	3.40(syn)	0.53	0.70	3.13(syn)	0.26	0.71		
Y I	39	2.21	-	-	-	2.77(syn)	0.56	0.94	2.42(syn)	0.21	0.38	2.49(syn)	0.28	0.73		
Y II	39	2.21	2.55±0.05(5)	0.34	0.11	3.20±0.08(9)	0.99	1.37	2.69±0.07(8)	0.48	0.65	2.51±0.09(3)	0.30	0.75		
Zr I	40	2.58	4.10(syn)	1.52	1.29	3.30(syn)	0.72	1.10	2.79(syn)	0.21	0.38	2.79(syn)	0.21	0.66		
Zr II	40	2.58	4.25(syn)	1.67	1.44	3.74(syn)	0.82	1.20	2.80(syn)	0.22	0.39	-	-	-		
Ba II	56	2.18	2.82(syn)	0.64	0.41	3.50(syn)	1.22	1.60	2.58(syn)	0.40	0.57	2.90(syn)	0.77	1.22		
La II	57	1.10	1.85(syn)	0.75	0.52	2.47(syn)	1.32	1.70	1.88(syn)	0.78	0.95	2.00(syn)	0.9	1.35		
Ce II	58	1.58	2.55±0.11(2)	0.97	0.74	2.92±0.16(14)	1.34	1.72	2.15±0.10(11)	0.57	0.74	2.70±0.20(10)	1.12	1.57		
Pr II	59	0.72	1.18±0.05(2)	0.46	0.23	1.93±0.11(3)	1.21	1.59	1.93±0.11(2)	1.21	1.59	1.54±0.18(3)	0.82	1.27		
Nd II	60	1.42	1.69±0.04(2)	0.27	0.04	2.66±0.10(19)	1.24	1.62	1.98±0.17(14)	0.56	0.73	2.10±0.12(10)	0.68	1.13		
Sm II	62	0.96	1.97±0.04(5)	1.01	0.78	2.62±0.17(8)	1.66	2.04	1.66±0.07(4)	0.70	0.87	2.09±0.18(7)	1.13	1.58		
Eu II	63	0.52	0.75(syn)	0.23	0.00	0.42(syn)	-0.10	0.28	0.48(syn)	-0.04	0.13	0.50(syn)	-0.02	0.43		

* Asplund (2009), The number inside the parenthesis shows the number of lines used for the abundance determination.

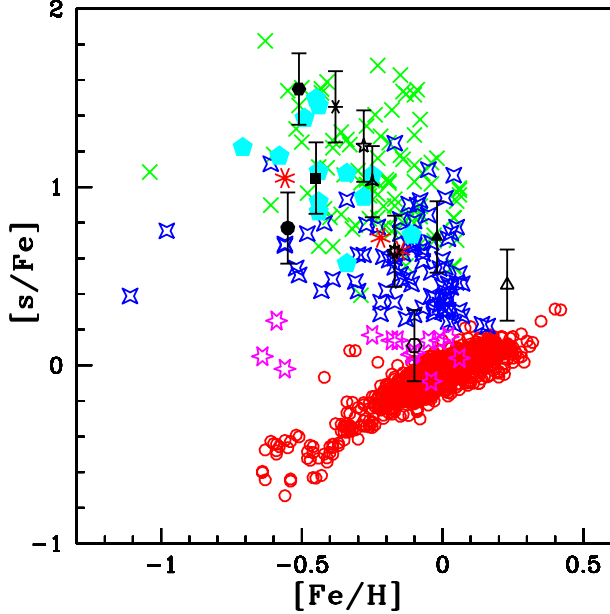


Figure 8. Observed $[s/Fe]$ ratios of the program stars with respect to metallicity $[Fe/H]$. Red open circles represent normal giants from literature (Luck & Heiter 2007). Green crosses, blue four-sided stars, cyan filled pentagons, red eight-sided crosses represent strong Ba giants, weak Ba giants, Ba dwarfs, Ba subgiants respectively from literature (de Castro et al. 2016, Yang et al. 2016, Allen & Barbuy 2006a). Magenta six-sided stars represent the stars rejected as Ba stars by de Castro et al. (2016). HD 24035 (filled hexagon), HD 32712 (starred triangle), HD 36650 (filled triangle), HD 94518 (filled circle), HD 147609 (five-sided star), HD 154276 (open hexagon), HD 179832 (open triangle), HD 207585 (six-sided cross), HD 211173 (nine-sided star) and HD 219116 (filled square).

els ($z = 0.0138$, $z = 0.006$ and $z = 0.003$), ^{13}C is only partially burned during the interpulse; surviving part is ingested in the convective zone generated by the subsequent thermal pulse (TP) and then burned at $T \sim 1.5 \times 10^8$ K, producing a neutron density of 10^{11} neutrons cm^{-3} . For larger z , $^{22}Ne(\alpha, n)^{25}Mg$ neutron source is marginally activated during the TPs; but for low z , it becomes an important source when most of the ^{22}Ne is primary (Cristallo et al. 2009, 2011). For the intermediate-mass AGB star models, the s-process distributions are dominated by the $^{22}Ne(\alpha, n)^{25}Mg$ neutron source, which is efficiently activated during TPs. The contribution from the $^{13}C(\alpha, n)^{16}O$ reaction is strongly reduced in the massive stars. This is due to the lower extent of the ^{13}C pocket in them. It is shown that the extent of ^{13}C pocket decreases with increasing core mass of the AGB, due to the shrinking and compression of He-intershell (Cristallo et al. 2009). These massive models experience Hot Bottom Burning and Hot-TDUs at lower metallicities (Cristallo et al. 2015b).

We have compared our observational data with the FRUITY model. The model predictions are unable to reproduce the $[hs/ls]$ ratios characterizing the surface composition of the stars. A comparison of the observed $[hs/ls]$ ratios with metallicity shows a large spread (Figure 10), somewhat similar to the comparison between the model and observational data as shown in Cristallo et al. (2011, Figure 12).

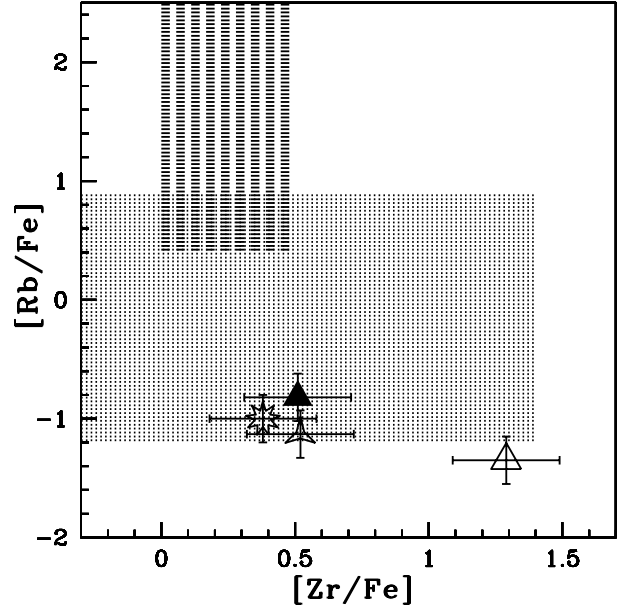


Figure 9. The observed abundances $[Rb/Fe]$ vs $[Zr/Fe]$. HD 32712 (starred triangle), HD 36650 (filled triangle), HD 179832 (open triangle), and HD 211173 (nine-sided star). The region shaded with short-dashed line and dots corresponds to the observed range of Zr and Rb in intermediate-mass and low-mass AGB stars respectively in the Galaxy and the Magellanic Clouds (van Raaij et al. 2012). The four stars occupy the region of low-mass AGB stars except for HD 179832 (open triangle) which lie marginally below this region.

The observed discrepancy may be explained considering different ^{13}C pocket efficiencies in the AGB models. In the FRUITY models a standard ^{13}C pocket is being considered, however, it needs to be checked if a variation in the amount of ^{13}C pocket would give a better match with the observed spread. Absence of stellar rotation in the current FRUITY models may also be a cause for the observed discrepancy. The rotation induced mixing alters the extend of ^{13}C pocket (Langer et al. 1999), which in turn affects the s-process abundance pattern. However, a study made by Cseh et al. (2018) using the rotating star models available for the metallicity range of Ba stars (Piersanti et al. 2013) could not reproduce the observed abundance ratios of stars studied in de Castro et al. (2016).

The observed abundance ratios for eight neutron-capture elements are compared with their counterparts in the low-mass AGB stars from literature, that are found to be associated with $^{13}C(\alpha, n)^{16}O$ neutron source (Figure 11). As discussed in de Castro et al. (2016) the scatter observed in the ratios may be a consequence of different dilution factors during the mass transfer, as well as the orbital parameters, metallicity and initial mass.

We have performed a parametric analysis in order to find the dilution experienced by the s-rich material after the mass transfer. The dilution factor, d , is defined as $M_{\star}^{env} / M_{AGB}^{transf} = 10^d$, where M_{\star}^{env} is the mass of the envelope of the observed star after the mass transfer, M_{AGB}^{transf} is the mass transferred from the AGB. The dilution factor is derived by comparing the observed abundance with the

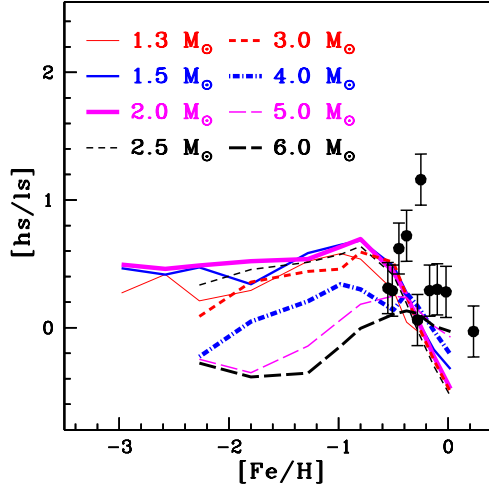


Figure 10. Comparison of predicted and observed values of $[hs/lis]$ ratios.

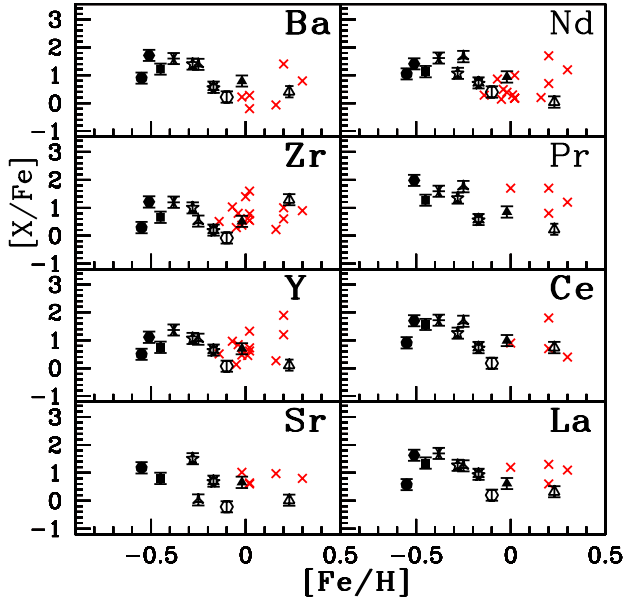


Figure 11. Comparison of abundance ratios of neutron-capture elements observed in the program stars and the AGB stars with respect to metallicity $[Fe/H]$. Red crosses represent the AGB stars from literature (Smith & Lambert 1985, 1986b, 1990, Abia & wallerstein 1998).

predicted abundance from FRUITY model for the heavy elements (Rb, Sr, Y, Zr, Ba, La, Ce, Pr, Nd, Sm and Eu). The solar values has been taken as the initial composition. The observed elemental abundances are fitted with the parametric model function (Husti et al. 2009). The best fits masses and corresponding dilution factors along with the χ^2 values are given in Table 9. The goodness of fit of the parametric model function is determined by the uncertainty in the observed abundance. The best fits obtained are shown in Figures 12 - 15. All the Ba stars are found to have low-

mass AGB companions with $M \leq 3 M_{\odot}$. Among our stars, HD 147609 is found to have a companion of $3 M_{\odot}$ by Husti et al. (2019), whereas our estimate is $2.5 M_{\odot}$.

6.7 Discussion on individual stars

HD 24035, HD 219116, HD 32712, HD 36650, HD 207585 and HD 211173:

These objects are listed in the CH star catalogue of Bartkevicius (1996) as well as in the barium star catalogue of Lü (1991). While Smith et al. (1993) classified HD 219116 as a CH subgiant, MacConnell et al. (1972) and Mennessier et al. (1997) suggested these objects to be giant barium stars. Based on our temperature and luminosity estimates, their locations in the H-R diagram correspond to the giant phase of evolution, except for HD 207585 which is found to be a strong Ba sub-giant. Earlier studies on these objects include Masseron et al. (2010) and de Castro et al. (2016) on abundance analysis. We have estimated the abundances of all the important s-process elements and Eu in these objects except Sr in HD 24035. Based on our abundance analysis we find these objects to satisfy the criteria for s-process enriched stars (Beers & Christlieb 2005) with $[Ba/Fe] > 1$ and $[Ba/Eu] > 0.50$ respectively. Following Yang et al. (2016), they can also be included in strong Ba giant category while HD 211173 is a mild Ba giant. They show the characteristics of Ba stars with estimated C/O $\sim 0.95, 0.51, 0.56, 0.24$ and 0.59 for HD 219116, HD 32712, HD 36650, HD 207585 and HD 211173 respectively. HD 24035 shows the largest enhancement of Ba among our program stars with $[Ba/Fe] \sim 1.71$ and largest mean s-process abundance with $[s/Fe] \sim 1.55$. A comparison with FRUITY models shows that the former AGB companions of HD 24035, HD 32712, HD 36650, HD 219116, HD 207585 and HD 211173 are low mass objects with masses $2.5 M_{\odot}, 2.0 M_{\odot}, 3.0 M_{\odot}, 3.0 M_{\odot}, 2.5 M_{\odot}$, and $2.5 M_{\odot}$ respectively. From kinematic analysis we find these objects to belong to the thin disk population with probability ≥ 0.97 . The estimated spatial velocities < 85 km/s, also satisfies the criterion of Chen et al. (2004) for stars to be thin disk objects. From radial velocity monitoring, HD 24035 and HD 207585 are confirmed to be binaries with orbital periods of 377.82 ± 0.35 days (Udry et al. 1998a) and 672 ± 2 days (Escorza et al. 2019) respectively.

HD 94518: This object belongs to the CH star catalogue of Bartkevicius (1996). Our abundance analysis places this object in the strong Ba star category with $C/O \sim 0.06$. The abundance pattern observed in this star resembles with that of a $1.5 M_{\odot}$ AGB star. The position of this stars in H-R diagram shows this object to be a subgiant star. Kinematic analysis shows this object to belong to thick disk population with a probability ~ 0.95 .

HD 147609: This star is listed in CH star catalogue of Bartkevicius (1996). This star is a strong Ba dwarf with $C/O \sim 0.27$. Comparison of the observed abundance in HD 147609 with the FRUITY model shows close resemblance with that seen in $2.5 M_{\odot}$ AGB star. Kinematic analysis has shown that this object belongs to thin disk population with characteristic spatial velocity of thin disk objects. The radial velocity monitoring study by Escorza et al. (2019) has confirmed this object to be a binary with an orbital pe-

Table 9. The best fitting mass, dilution factor and reduced chi-square values.

Star name/ mass (M/M_{\odot})		HD 24035	HD 32712	HD 36650	HD 94518	HD 147609	HD 154276	HD 179832	HD 207585	HD 211173	HD 219116
1.5	d	-	-	-	0.22	-	0.71	0.21	-	-	0.04
	χ^2	-	-	-	9.91	-	1.46	51.39	-	-	1.40
2.0	d	-	0.001	-	0.52	-	1.18	0.65	-	-	0.36
	χ^2	-	16.14	-	10.14	-	1.43	48.04	-	-	1.55
2.5	d	0.07	0.08	0.10	0.62	0.08	1.31	0.82	0.07	0.03	0.46
	χ^2	1.92	17.64	8.15	10.31	1.39	1.60	48.06	4.28	18.15	1.66
3.0	d	-	-	0.04	0.27	-	1.20	0.75	-	-	0.10
	χ^2	-	-	8.08	9.92	-	1.52	48.01	-	-	1.33
4.0	d	-	-	-	-	-	0.58	-	-	-	-
	χ^2	-	-	-	-	-	1.01	-	-	-	-
5.0	d	-	-	-	-	-	0.09	-	-	-	-
	χ^2	-	-	-	-	-	0.91	-	-	-	-

riod of 1146 ± 1.5 days.

HD 154276: This star is listed in CH star catalogue of Bartkevicius (1996). Our analysis have shown that this star is a dwarf. Our analysis based on mean s-process abundance, $[s/Fe]$, revealed that this object can not be considered as a Ba star.

HD 179832: This object belongs to the CH star catalogue of Bartkevicius (1996). We have presented a first time detailed abundance analysis for this object. Our analyses have shown that this object is a mild Ba giant. The abundance trend observed in this star suggest that the former companion AGB star’s mass to be $3 M_{\odot}$. From kinematic analysis, HD 179832 is found to be a thin disk object with probability of 0.99. The spatial velocity is estimated to be 11.97 km s^{-1} , as expected for thin disk stars (Chen et al. 2004).

7 CONCLUSIONS

Results from high resolution spectroscopic analysis of ten objects are presented. All the objects are listed in the CH star catalog of Bartkevicius (1996). Six of them are also listed in the barium star catalog of Lü (1991). Except for one object HD 154276, all other objects are shown to be bonafied barium stars from our analysis. Although it satisfies the criteria of Yang et al. (2016) to be a mild barium star, our detailed abundance analysis shows this object to be a normal metal-poor star. An analysis based on the mean s-process abundance clearly shows that this particular star lies among the stars rejected as barium stars by de Castro et al. (2016).

Some of the objects analysed here, although common to the sample analysed by different authors, abundances of important heavy elements such as Rb, and C, N, O are not found in literature. New results for these elements are presented in this work.

We have presented first time abundance results for HD 179832 and shown it to be a mild barium giant. Kinematic analysis have shown it to be a thin disk object. A parametric model based analysis have shown the object’s former companion AGB star’s mass to be about $3M_{\odot}$.

The sample of stars analysed here covers a metallicity range from -0.55 to $+0.23$, and a kinematic analysis has shown that all of them belong to the Galactic disk, as expected for barium stars.

The estimated mass of the barium stars are consistent with that observed for other barium stars (Allen & Barbuy 2006a, Liang et al. 2003, Antipova et al. 2004, de Castro et al. 2016). The abundance estimates are consistent with the operation of $^{13}\text{C}(\alpha, n)^{16}\text{O}$ source in the former low-mass AGB companion.

We did not find any enhancement of Mg in our sample, that discards the source of neutron as the $^{22}\text{Ne}(\alpha, n)^{25}\text{Mg}$ reaction. An enhancement of Mg abundances when compared with their counterparts in disk stars and normal giants would have indicated the operation of $^{22}\text{Ne}(\alpha, n)^{25}\text{Mg}$.

The detection of Rb I line at 7800.259 \AA in the spectra of HD 32712, HD 36650, HD 179832 and HD 211173 allowed us to determine $[Rb/Zr]$ ratio. This ratio gives an indication of the neutron source at the s-process site and in turn provides clues to the mass of the star. We have obtained negative values for this ratio in all the four stars. The negative values obtained for these stars indicate the operation of $^{13}\text{C}(\alpha, n)^{16}\text{O}$ reaction. As this reaction occurs in the low-mass AGB stars, we confirm that the former companions of these stars are low-mass AGB stars with $M \leq 3 M_{\odot}$.

Distribution of abundance patterns and $[hs/ls]$ ratios also indicate low-mass companions for the objects for which $[Rb/Zr]$ could not be estimated. A comparison of observed abundances with the predictions from FRUITY models, and with those that are observed in low-mass AGB stars from literature, confirms low-mass for the former companion AGB stars.

8 ACKNOWLEDGMENT

We thank the staff at IAO and at the remote control station at CREST, Hosakotte for assisting during the observations. Funding from the DST SERB project No. EMR/2016/005283 is gratefully acknowledged. This work made use of the SIMBAD astronomical database, operated at CDS, Strasbourg, France, and the NASA ADS, USA. This work has made use of data from the European Space Agency (ESA) mission

Table 10. Comparison of the heavy elemental abundances of our program stars with the literature values.

Star name	[Fe I/H]	[Fe II/H]	[Fe/H]	[Rb I/Fe]	[Sr/Fe]	[Y I/Fe]	[Y II/Fe]	[Zr I/Fe]	Ref
HD 24035	-0.51	-0.50	-0.51	-	-	1.61	-	1.21	1
	-0.23	-0.28	-0.26	-	-	1.35	-	1.20	2
	-	-	-0.14	-	-	-	-	-	3
HD 32712	-0.25	-0.25	-0.25	-1.13	0.03	0.56	1.04	0.52	1
	-0.24	-0.25	-0.25	-	-	0.74	-	0.56	2
HD 36650	-0.02	-0.02	-0.02	-0.82	0.66	0.51	0.70	0.51	1
	-0.28	-0.28	-0.28	-	-	0.55	-	0.46	2
HD 94518	-0.55	-0.55	-0.55	-	1.18	-	0.50	-	1
	-0.49	-0.50	-0.50	-	0.55	-	-	-	4
HD 147609	-0.28	-0.28	-0.28	-	1.51	-	1.07	-	1
	-0.45	+0.08	-0.45	-	1.32	-	1.57	0.89	5
	-	-	-	-	-	0.96	-	0.80	6
HD 154276	-0.09	-0.10	-0.10	-	-0.22	-	0.07	-	1
	-	-	-0.29	-	-	-0.07	-	-	4
HD 179832	+0.23	+0.23	+0.22	-1.35	0.02	-	0.11	1.29	1
HD 207585	-0.38	-0.38	-0.38	-	-	0.94	1.37	1.10	1
	-	-	-0.50	-	-	-	-	-	3
	-	-	-0.57	-	-	1.29	-	1.50	7
HD 211173	-0.17	-0.17	-0.17	-1.00	0.70	0.38	0.65	0.38	1
	-	-	-0.12	-	-	-	-	-	3
HD 219116	-0.45	-0.44	-0.45	-	0.71	0.73	0.75	0.66	1
	-0.61	-0.62	-0.62	-	-	0.59	-	0.65	2
	-	-	-0.34	-	-	-	-	-	3
	-	-	-0.30	-	-	-	-	-	8
Star name	[Zr II/Fe]	[Ba II/Fe]	[La II/Fe]	[Ce II/Fe]	[Pr II/Fe]	[Nd II/Fe]	[Sm II/Fe]	[Eu II/Fe]	Ref
HD 24035	1.89	1.71	1.63	1.70	1.98	1.41	2.03	0.19	1
	-	-	2.70	1.58	-	1.58	-	-	2
	-	1.07	1.01	1.63	-	-	-	0.32	3
HD 32712	0.82	1.39	1.25	1.68	1.67	1.76	1.71	0.04	1
	-	-	1.53	1.16	-	1.19	-	-	2
HD 36650	-	0.79	0.62	0.99	0.85	0.94	0.99	-0.21	1
	-	-	0.83	0.68	-	0.57	-	-	2
HD 94518	0.29	0.90	0.58	0.91	-	1.05	1.39	-0.17	1
	-	0.77	-	-	-	-	-	-	4
HD 147609	1.00	1.40	1.27	1.26	1.35	1.07	1.29	0.13	1
	1.56	1.57	1.63	1.64	1.22	1.32	1.09	0.74	5
	-	-	-	-	-	0.98	-	-	6
HD 154276	-0.08	0.22	0.20	0.18	-	0.40	0.07	-	1
	-	-0.03	-	-	-	-	-	-	4
HD 179832	1.44	0.41	0.52	0.74	0.23	0.04	0.78	0.00	1
HD 207585	1.20	1.60	1.70	1.72	1.59	1.62	2.04	-0.02	1
	-	1.23	1.37	1.41	-	-	-	0.58	3
	-	-	1.60	0.84	0.61	0.93	1.05	-	7
HD 211173	0.39	0.57	0.95	0.74	1.59	0.73	0.87	-0.17	1
	-	0.35	0.29	0.73	-	-	-	0.15	3
HD 219116	-	1.22	1.35	1.57	1.27	1.13	1.58	0.13	1
	-	-	1.21	1.07	-	-	-	-	2
	-	0.77	0.56	0.80	-	-	-	0.17	3
	-	0.90	-	-	-	1.43	-	-	8

References: 1. Our work, 2. de Castro (2016), 3. Masseron et al. (2010), 4. Bensby et al. (2014), 5. Allen & Barbuy (2006a), 6. North et al. (1994a), 7. Luck & Bond (1991), 8. Smith et al. (1993)

Gaia (<https://www.cosmos.esa.int/gaia>), processed by the Gaia Data Processing and Analysis Consortium (DPAC, <https://www.cosmos.esa.int/web/gaia/dpac/consortium>). T.M. acknowledges support provided by the Spanish Ministry of Economy and Competitiveness (MINECO) under grant AYA- 2017-88254-P. Based on data collected using HESP, UVES and FEROS. The authors would like to thank the referee for useful suggestions that had improved the readability of the paper.

REFERENCES

- Abbondanno U., Aerts G., Alvarez-Velarde F., Ivarez-Pol H., Andriamonje S. et al., 2004, *Phys. Rev. Lett.*, 93, 1103
- Abia C., Wallerstein G., 1998, *MNRAS*, 293, 89
- Abia C., Busso M., Gallino R., Domínguez I., Straniero O. & Isern J., 2001, *ApJ*, 559, 1117
- Afsar M., Sneden C., For B -Q., 2012, *AJ*, 144, 20
- Alonso A., Arribas S., Martínez-Roger C., 1994, *A&ASS*, 107, 365
- Alonso A., Arribas S., Martínez-Roger C., 1995, *A&A*, 297, 197
- Alonso A., Arribas S., Martínez-Roger C., 1996, *A&A*, 313, 873
- Alonso A., Arribas S., Martínez-Roger C., 1999, *A&AS*, 140, 261
- Alonso A., Arribas S., Martínez-Roger C., 2001, *A&A*, 376, 1039
- Allen D.M., Barbuy B., 2006a, *A&A*, 454, 895
- Amarsi A. M., Asplund M., Collet R. & Leenaarts, J., 2016, *MNRAS*, 455, 3735
- Antipova L.I., Boyarchuk A.A., Pakhomov Yu. V. & Panchuk V.E., 2004, *ARep*, 48, 597
- Asplund M., Grevesse N., Sauval A.J., 2009, *Ann. Rev. Astron. Astrophys.*, 47, 481
- Axer M., Fuhrmann K., Gehren T., 1994, *A&A*, 291, 895
- Barbuy B., Jorissen A., Rossi S. C. F. & Arnould M., 1992, *A&A*,

Table 11. Equivalent widths (in mÅ) of Fe lines used for deriving atmospheric parameters.

Wavelength(Å)	El	E_{low} (eV)	log gf	HD 24035	HD 32712	HD 36650	HD 94518	HD 147609	HD 154276	HD 179832	HD 207585	HD 211173	HD 219116	Ref
4114.445	Fe I	2.832	-1.220	-	-	-	-	-	-	-	-	-	-	1
4132.899		2.850	-1.010	-	-	-	88.7(6.94)	-	-	-	83.4(6.96)	132.2(7.31)	-	1
4153.900		3.400	-0.320	129.9(6.79)	-	-	-	-	-	-	90.8(6.90)	-	-	1
4154.499		2.830	-0.690	-	-	-	-	-	-	-	-	-	-	2
4184.891		2.832	-0.860	-	-	-	-	-	-	-	-	-	-	1

The numbers in the paranthesis in columns 5-14 give the derived abundances from the respective line.

References: 1. Führ et al. (1988) 2. Kurucz (1988)

Note: This table is available in its entirety in online only. A portion is shown here for guidance regarding its form and content.

Table 12. Equivalent widths (in mÅ) of lines used for deriving elemental abundances.

Wavelength(Å)	El	E_{low} (eV)	log gf	HD 24035	HD 32712	HD 36650	HD 94518	HD 147609	HD 154276	HD 179832	HD 207585	HD 211173	HD 219116	Ref
5682.633	Na I	2.102	-0.700	126.7(6.29)	133.5(6.31)	126.0(6.44)	63.5(5.86)	66.2(6.13)	83.5(6.23)	132.2(6.55)	79.0(6.17)	121.5(6.43)	104.5(6.13)	1
5688.205		2.105	-0.450	137.1(6.21)	151.3(6.31)	130.1(6.26)	85.2(5.94)	98.2(6.39)	-	145.1(6.50)	98.0(6.22)	136.2(6.41)	126.8(6.24)	1
6154.226		2.102	-1.560	49.4(5.91)	66.9(6.04)	67.7(6.30)	20.5(5.90)	-	27.4(6.13)	-	22.2(6.00)	60.1(6.21)	37.9(5.92)	1
6160.747		2.104	-1.260	88.3(6.20)	92.7(6.16)	87.5(6.31)	29.2(5.81)	-	47.9(6.22)	-	38.0(6.03)	74.8(6.15)	57.2(5.93)	1
4571.096	Mg I	0.000	-5.691	-	-	-	-	-	108.9(7.88)	-	-	-	-	2
4702.991		4.346	-0.666	-	179.6(7.10)	-	179.6(7.27)	156.2(7.56)	-	-	149.0(7.16)	-	180.0(7.48)	3
4730.029		4.346	-2.523	-	-	85.1(7.71)	45.5(7.46)	32.3(7.48)	60.2(7.80)	87.1(7.81)	-	76.8(7.60)	-	3

The numbers in the paranthesis in columns 5-14 give the derived abundances from the respective line.

References: 1. Kurucz et al. (1975), 2. Laughlin et al. (1974), 3. Lincke et al. (1971)

Note: This table is available in its entirety in online only. A portion is shown here for guidance regarding its form and content.

- 262, 216
- Bartkevicius A., 1996, *Baltic Astron*, 5, 217
- Baschek B., Scholz M. & Sedlmayr E., 1977, *A&A*, 55, 375
- Battistini C. & Bensby T., 2015, *A&A*, 577, 9
- Beer H., 1991, *ApJ*, 375, 823
- Beers T.C., Christlieb N., 2005, *ARA&A*, 43, 531
- Beer H. & Macklin R. L., 1989, *ApJ*, 339, 962
- Bensby T., Feltzing S., Lundstrom I., 2004, *A&A*, 415, 155
- Bensby T., Feltzing S., Oey M.S., 2014, *A&A*, 562, 71
- Bidelman W.P., Keenan P.C., 1951, *ApJ*, 114, 473
- Boyarchuk A.A., Antipova L.I., Boyarchuk M.E. & Savanov I.S., 2001, *ARep*, 45, 301
- Brooke J. S. A., Bernath P. F., Schmidt T. W. & Bacskay G. B., 2013, *JQSRT*, 124, 11
- Busso M., Gallino R., Wasserburg G. J., 1999, *ARA&A*, 37, 239
- Busso M., Gallino R., Lambert D. L., Travaglio C., Smith V. V., 2001, *ApJ*, 557, 802
- Cenarro A.J., Peletier R.F., Sanchez-Blazquez P., selam S.O., Toloba E., Cardiel N., Falcon - Barroso J., Gorgas J., Jimenez-Vicente & Vazdekis A., 2007, *MNRAS*, 374, 664
- Chen B., Vergely J.L., Valette B., Carraro G., 1998, *A&A*, 336, 137
- Chen Y.Q., Nissen P.E., Zhao G., 2004, *A&A*, 425, 697
- Clayton D. D., 1988, *MNRAS*, 234, 1
- Cristallo S., Straniero O., Gallino R., Piersanti L., Domínguez I., Lederer M. T., 2009, *ApJ*, 696, 797
- Cristallo S., Piersanti L., Straniero O., Gallino R., Domínguez I., Abia C., di rico G., Quintini M., Bisterzo S., 2011, *ApJS*, 197, 17
- Cristallo S., Straniero O., Piersanti L. & Gobrecht D., 2015b, *ApJS*, 219, 40
- Cseh B., Lugaro M., D’Orazi V., de Castro D. B., Pereira C.B., Karakas A. I. et al., 2018, *A&A*, 620, A146
- Cutri R.M., Skrutskie M.F., Van Dyk S., Beichman C A., Carpenter J.M, 2003, *yCat*.2246.0
- de Castro D.B., Pereira C.B., Roig F., Jilinski E., Drake N.A., Chavero C., Sales Silva J.V., 2016, *MNRAS*, 459, 4299
- Denissenkov P.A. & Ivanov V.V., 1987, *SvAL*, 13, 214
- Doherty C. L., Gil-Pons P., Lau H. H. B., Lattanzio J. C & Siess L., 2014a, *MNRAS*, 437, 195
- Dray L. M., tout C. A., Karakas A. I., Lattanzio J. C., 2003, *MNRAS*, 338, 973
- Edvardsson B., Andersen J., Gustafsson B., Lambert D.L., Nissen P. E., Tomkin J., 1993, *A&A*, 275, 101
- El Eid M.F. & Champagne A.E., 1995, *ApJ*, 451, 298
- Eriksson K. & Toft S. C., 1979, *A&A*, 71, 178
- Escorza A., Karinkuzhi D., Jorissen A., Siess L., Van Winckel H. et al., 2019, *A&A*, 626, A128
- Führ J.R., Martin G.A., Wiese W.L., 1988, *J. Phys. Chem. Ref. Data* 17, Suppl. 4
- Gallino R., Arlandini C., Busso M., Lugaro M., Travaglio C., Straniero O., Chieffi A., Limongi M., 1998, *ApJ*, 497, 388
- García-Herández D. A., García-Lario P., Plez B., D’Antona F., Manchado A., Trigo-Rodríguez M., 2006, *Science*, 314, 1751
- García-Herández D. A., García-Lario P., Plez B., Manchado A., D’Antona F., Lub J. & Habing H., 2007, *A&A*, 462, 711
- García-Herández D. A., Manchado A., Lambert D. L., Plez B., García-Lario P., D’Antona F., Lugaro M., Karakas A. I. & van Raai M. A., 2009, *ApJ*, 705, L31
- Girardi L., Bressan A., Bertelli G., Chiosi C., 2000, *A&AS* 141, 371
- Goriely S., Mowlavi N., 2000, *A&A*, 362, 599
- Görres J., Arlandini C., Giesen U., Heil M., Käppeler F., Leiste H., Stech E., Wiescher M., 2000, *Phys. Rev. C*, 62, 5801
- Goswami A., Aoki W., Beers T. C., Christlieb N., Norris J. E., Ryan S. G., Tsangarides S., 2006, *MNRAS*, 372, 343
- Goswami A., Aoki W., Karinkuzhi D., 2016, *MNRAS*, 455, 402
- Harris M. J., Lambert D. L. & Smith V. V., 1985, *ApJ*, 292, 620
- Heil M., Käppeler F., Uberseder E., Gallino R., bisterzo S., Pignatari M., 2008a, *Phys. Rev. C*, 78, 5802
- Heil M., Winckler N., Dababneh S., Kppeler F., Wisshak K., Bisterzo S., Gallino R., Davis A. M., Rauscher T., 2008b, *ApJ*, 673, 434
- Henry R. B. C., Edmunds M. G., Köppen J., 2000, *ApJ*, 541, 660
- Herwig F., 2005, *ARA&A*, 43, 435
- Husti L., Gallino R., Bisterzo S., Straniero O. & Cristallo S., 2009, *PASA*, 26, 176
- Iben Jr. I., 1975, *ApJ*, 196, 525
- Jaeger M., Kunz R., Mayer A., Hammer J. W., Staudt G., Kratz K. L., Pfeiffer B., 2001, *Phys. Rev. Lett.*, 87, 2501
- Johnson H.R., Milkey R.W., Ramsey L.W., 1974, *ApJ*, 187, 147
- Jonsell K., Barklem P. S., Gustafsson B., Christlieb N., Hill V., Beers T. C., Holmberg J., 2006, *A&A*, 451, 651
- Karakas A. I., Lattanzio J. C., 2014, *PASA*, 31, 30
- Karakas A.I., García-Hernández D. A. & Lugaro M., 2012, *ApJ*, 751, 8

Table 13. Estimates of [ls/Fe], [hs/Fe], [s/Fe], [hs/ls], [Rb/Sr], [Rb/Zr], C/O

Star name	[Fe/H]	[ls/Fe]	[hs/Fe]	[s/Fe]	[hs/ls]	[Rb/Sr]	[Rb/Zr]	C/O
HD 24035	-0.51	1.41	1.61	1.55	0.20	-	-	-
HD 32712	-0.25	0.37	1.52	1.03	1.15	-1.06	-1.65	0.51
HD 36650	-0.02	0.56	0.84	0.72	0.28	-1.48	-1.33	0.56
HD 94518	-0.55	0.67	0.86	0.77	0.19	-	-	0.06
HD 147609	-0.28	1.19	1.25	1.23	0.06	-	-	0.27
HD 154276	-0.10	-0.08	0.25	0.11	0.33	-	-	-
HD 179832	+0.23	0.47	0.66	0.45	0.19	-1.37	-2.64	-
HD 207585	-0.38	1.02	1.66	1.45	0.64	-	-	0.24
HD 211173	-0.17	0.49	0.75	0.64	0.26	-1.70	-1.38	0.59
HD 219116	-0.45	0.70	1.32	1.05	0.62	-	-	0.95

- Karinkuzhi D., Van Eck S., Jorissen A., Goriely S., Siess L., Merle T., Escorza A., Van der Swaelmen M., Boffin H. M. J., Masseron T., Shetye S. & Plez B., 2018, *A&A*, 618, A32
- Keenan P.C., 1942, *ApJ*, 96, 101
- Kiselman D., 1993, *A&A*, 275, 269
- Kurucz R.L., 1988, *Trans. IAU, XXB*, M. McNally, ed., *Dordrecht: Kluwer*, 168-172
- Kurucz R.L., Peytremann E., 1975, *SAO Special Report* 362
- Lambert D. L. & Luck R. E., 1976, *Obs.*, 96, 100L
- Lambert D. L., Smith V. V., Busso M., Gallino R. & Straniero O., 1995, *ApJ*, 450, 302
- Langer N., Heger A., Wellstein S. & Herwig F., 1999, *A&A*, 346, L37
- Laughlin C., Victor G.A., 1974, *ApJ* 192, 551
- Liang Y.C., Zhao G., Chen Y.Q. & Qiu H.M. & Zhang B., 2003, *A&A*, 397, 257
- Lincke R., Ziegenbein G., 1971, *Z. Physik*, 241, 369.
- Lü P.K., 1991, *AJ*, 101, 2229
- Lucatello S., Tsangarides S., Beers T. C., Carretta E., Gratton R. G., Ryan S. G., 2005, *ApJ*, 652, 825
- Luck R.E. & Bond H.E., 1991, *ApJS*, 77, 515
- Luck R. E. & Heiter U., 2007, *AJ*, 133, 2464
- Luck R. E. & Lambert D. L., 1985, *ApJ*, 298, 782
- Lugaro M. & Chieffi A., 2011, in *Lecture Notes in Physics*, ed. R. Diehl, D. H. Hartmann & N. Prantzos (Berlin: Springer Verlag), 812, 83
- MacConnell D.J., Frye R.L., Upgren A.R., 1972, *AJ*, 77, 384
- Masseron T., Johnson J.A., Plez B., Van Eck S., Goriely S., Jorissen A., 2010, *A&A*, 509, 93
- McClure R.D., 1983, *ApJ*, 208, 264
- McClure R.D., 1984, *ApJ*, 280, 31
- McClure R.D., Woodsworth W., 1990, *ApJ*, 352, 709
- McClure R. D., Fletcher J. M., Nemeč J., 1980, *ApJ*, 238, L35
- McWilliam A., 1998, *AJ*, 115, 1640
- Mennessier M.O., Luri X., Figueras F., Gomez A.E., Grenier S. et al., 1997, *A&A*, 326, 722
- Merle T., Jorissen A., Van Eck S., Masseron T. & Van Winckel H., 2016, *A&A*, 586, A151
- Mishenina T.V., Bienaym O., Gorbaneva T.I., Charbonnel C., 2006, *A&A*, 456, 1109
- Mowlavi N., 1999, *A&A*, 344, 617
- North P., Berthet S., Lanz T., 1994a, *A&A*, 281, 775
- Patronis N., Dababneh S., Assimakopoulos P. A., Gallino R., Heil M., Käppeler F., Karamanis D., Koehler P. E., Mengoni A., Plag R., 2004, *Phys. Rev. Lett.*, 69, 5803
- Piersanti L., Cristallo S. & Straniero O., 2013, *ApJ*, 774, 98
- Pilachowski C.A., 1977, *A&A*, 54, 465
- Plez B., Smith V. V. & Lambert D. L., 1993, *ApJ*, 418, 812
- Prochaska J.X., McWilliam A., 2000, *ApJ*, 537, 57
- Prochaska J. X., Naumov S. O., Carney B. W., McWilliam A., Wolfe A. M., 2000, *AJ*, 120, 2513
- Purandardas M., Goswami A., Goswami P. P., Shejeelammal J., Masseron T., 2019, *MNRAS*, 486, 3266
- Ramirez I., feltzing S. & Oey M. S., 2013, *ApJ*, 764, 78
- Ram R. S., Brooke James S. A., Bernath P. F., Sneden C., Lucatello S., 2014, *ApJS*, 211, 5
- Reddy B.E., Tomkin J., Lambert D.L. & Allende Prieto C., 2003, *MNRAS*, 340, 304
- Reddy B.E., Lambert D.L., Prieto C.A., 2006, *MNRAS*, 367, 1329
- Rojas M., Drake N. A., Pereira C. B. & Kholtygin A. F., 2013, *Astrophysics*, 56, 57
- Smiljanic R., Barbuy B., de Medeiros J. R., Maeder A., 2006, *RMxAC*, 26, 45
- Smiljanic R., Porto de Mello G. F., da Silva L., 2007, *A&A*, 468, 679
- Smith V. V., 1984, *A&A*, 132, 326
- Smith V. V., Lambert D. L., 1985, *ApJ*, 294, 326
- Smith V. V. & Lambert D. L., 1986a, *ApJ*, 303, 226
- Smith V. V., Lambert D. L., 1986b, *ApJ*, 311, 843
- Smith V. V., Lambert D. L., 1990, *ApJS*, 72, 387
- Smith V. V., Coleman H. & Lambert D. L., 1993, *ApJ*, 417, 287
- Sneden C., 1973, *PhD thesis*, Univ. Texas
- Sneden C., Pilachowski C. A. & Lambert D. L., 1981, *ApJ*, 247, 1052
- Sneden C., Lucatello S., Ram R. S., Brooke J. S. A. & Bernath P. F., 2014, *ApJS*, 214, 26
- Stancliffe R.J., Glebbeek E., Izzard R.G., Pols O.R., 2007, *A&A*, 464, 57
- Straniero O., Gallino R., Busso M., Chieffi A., Raiteri C. M., Limongi M., Salaris M., 1995, *ApJ*, 440, L85
- Straniero O., Gallino R. & Cristallo S., 2006, *Nucl. Phys. A*, 777, 311
- Thévenin F. & Idiart T. P., 1999, *ApJ*, 521, 753
- Tomkin J. & Lambert D. L., 1979, *ApJ*, 227, 209
- Tomkin J. & Lambert D. L., 1983, *ApJ*, 273, 722
- Udry S., Jorissen A., Mayor M., Van Eck S., 1998a, *A&AS*, 131, 25
- Udry S., Mayor M., Van Eck S., Jorissen A., Prévot L., Grenier S., Lindgren H., 1998b, *A&AS*, 131, 43
- van Raai M. A., Lugaro M., Karakas A. I., García-Hernández D. A. & Yong D., 2012, *A&A*, 540, A44
- Vanture A.D., 1992, *AJ*, 104, 1977
- Wallerstein G., 1997, *RvMP*, 69,995
- Woosley S. E. & Weaver T. A., 1995, *ApJS*, 101, 181
- Worely C.C., Hill V. J., Sobeck J., Carretta E., 2013, *A&A*, 553, A47
- Yang G.C., Liang Y.C., Spite M., Chen Y.Q., Zhao G. et al., 2016, *RAA*, 16, 1

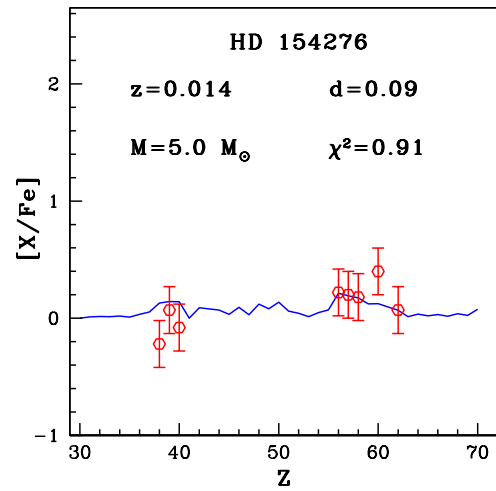
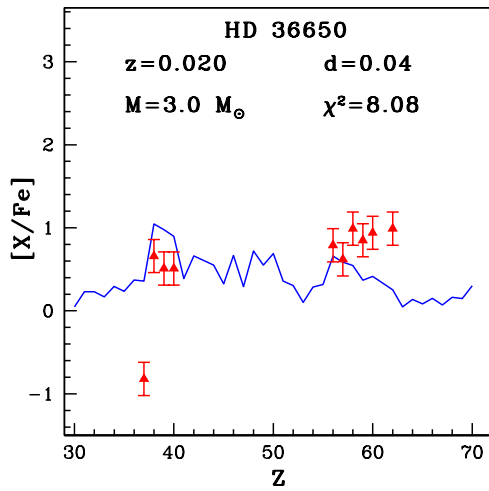
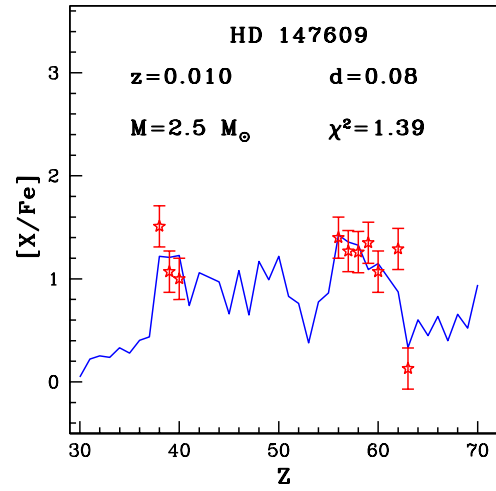
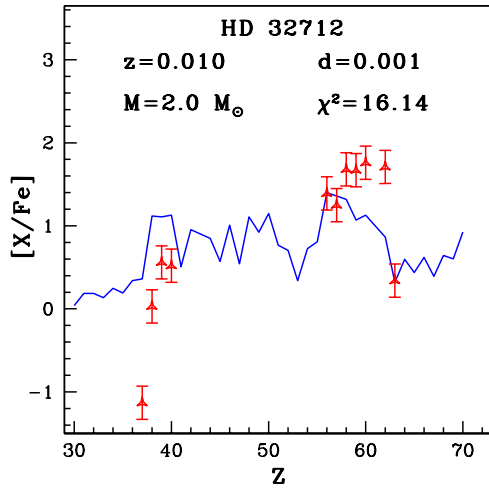
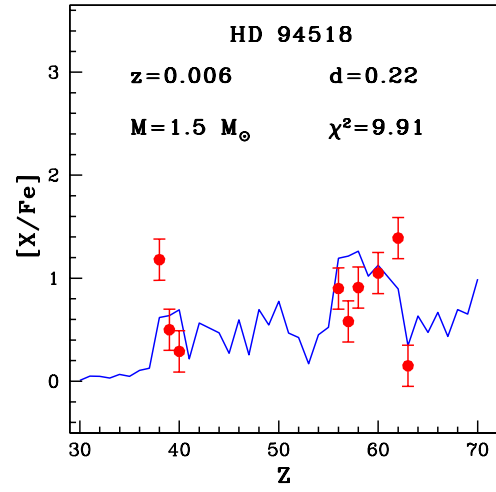
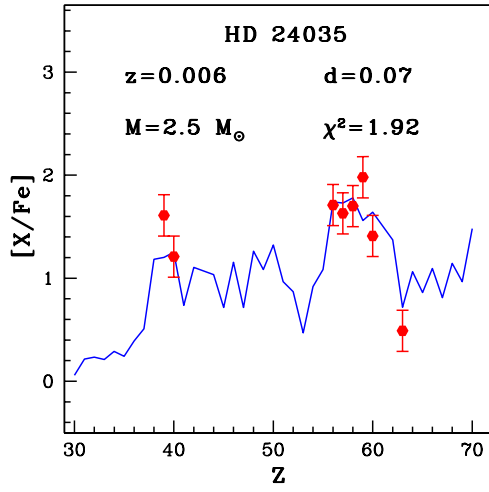


Figure 12. Solid curve represent the best fit for the parametric model function. The points with error bars indicate the observed abundances in (i) *Top panel:* HD 24035 (ii) *Middle panel:* HD 32712 (iii) *Bottom panel:* HD 36650.

Figure 13. Solid curve represent the best fit for the parametric model function. The points with error bars indicate the observed abundances in (i) *Top panel:* HD 94518 (ii) *Middle panel:* HD 147609 (iii) *Bottom panel:* HD 154276.

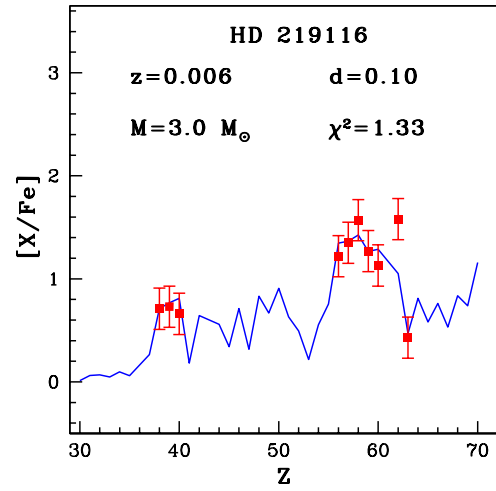
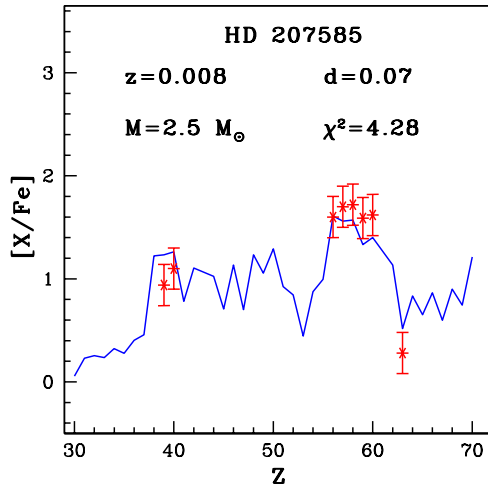
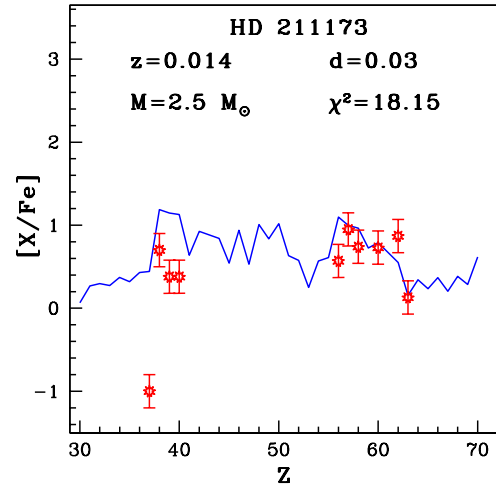
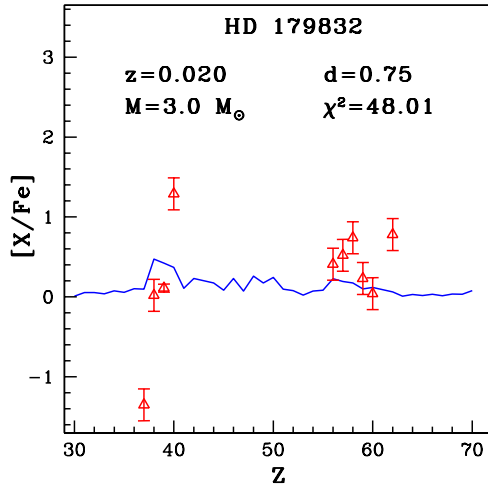


Figure 14. Solid curve represent the best fit for the parametric model function. The points with error bars indicate the observed abundances in (i) *Top panel*: HD 179832 (ii) *Bottom panel*: HD 207585.

Figure 15. Solid curve represent the best fit for the parametric model function. The points with error bars indicate the observed abundances in (i) *Top panel*: HD 211173 (ii) *Bottom panel*: HD 219116.

APPENDIX

Table 14. Spatial velocity and probability estimates for the program stars

Star name	U_{LSR} (kms^{-1})	V_{LSR} (kms^{-1})	W_{LSR} (kms^{-1})	V_{spa} (kms^{-1})	P_{thin}	P_{thick}	P_{halo}	Population
HD 24035	-11.18 ± 0.52	27.32 ± 0.38	-16.35 ± 0.58	33.74 ± 0.15	0.99	0.01	0.00	Thin disk
HD 32712	76.78 ± 0.66	-11.17 ± 0.16	17.13 ± 0.17	79.46 ± 0.65	0.97	0.03	0.00	Thin disk
HD 36650	21.44 ± 0.13	-18.64 ± 0.17	-10.09 ± 0.13	30.15 ± 0.06	0.99	0.01	0.00	Thin disk
HD 94518	46.24 ± 0.11	-119.85 ± 0.43	-62.49 ± 0.44	142.85 ± 0.52	0.00	0.95	0.05	Thick disk
HD 147609	19.45 ± 0.87	-15.64 ± 0.90	-4.11 ± 1.03	25.30 ± 0.06	0.99	0.01	0.00	Thin disk
HD 154276	1.75 ± 0.96	-116.16 ± 0.76	22.48 ± 0.76	118.33 ± 0.58	0.07	0.92	0.01	Thick disk
HD 179832	9.21 ± 0.15	-5.80 ± 0.32	-4.98 ± 0.21	11.97 ± 0.41	0.99	0.01	0.00	Thin disk
HD 207585	-27.10 ± 0.32	-41.91 ± 2.68	44.05 ± 1.04	66.57 ± 1.13	0.72	0.28	0.00	Thin disk
HD 211173	-48.53 ± 0.88	27.71 ± 0.42	4.79 ± 0.54	56.09 ± 0.51	0.99	0.01	0.00	Thin disk
HD 219116	-46.22 ± 1.31	-17.18 ± 0.49	25.18 ± 0.59	55.37 ± 0.98	0.97	0.03	0.00	Thin disk

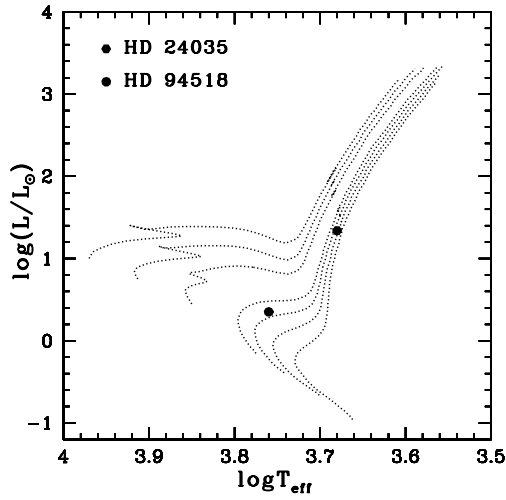


Figure 16. The locations of HD 24035 and HD 94518. The evolutionary tracks for 0.6, 0.7, 0.8, 0.9, 1.2, 1.4, and 1.6 M_{\odot} are shown from bottom to top for $z = 0.004$.

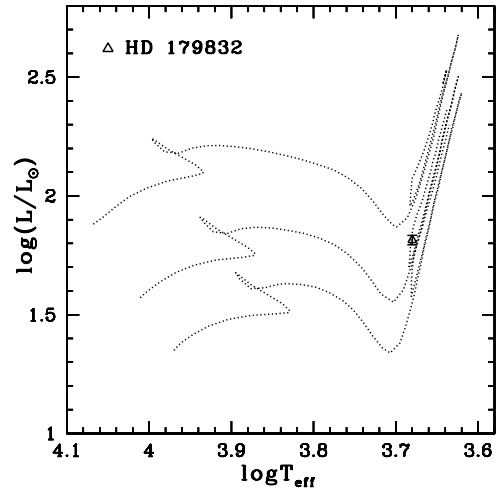


Figure 18. The location of HD 179832. The evolutionary tracks for 2.2, 2.5, and 3.0 M_{\odot} are shown from bottom to top for $z = 0.030$.

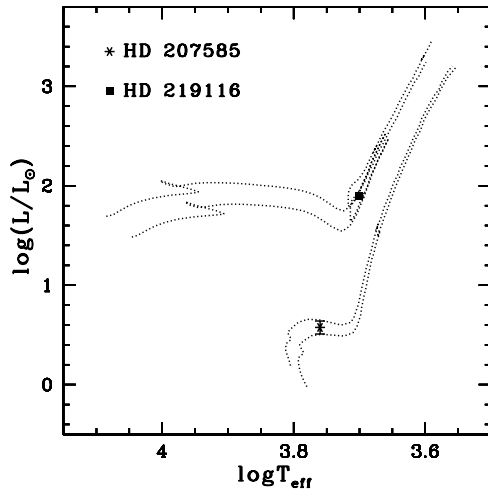


Figure 17. The locations of HD 207585 and HD 219116. The evolutionary tracks for 1.0, 1.1, 2.2, and 2.5 M_{\odot} are shown from bottom to top for $z = 0.008$.

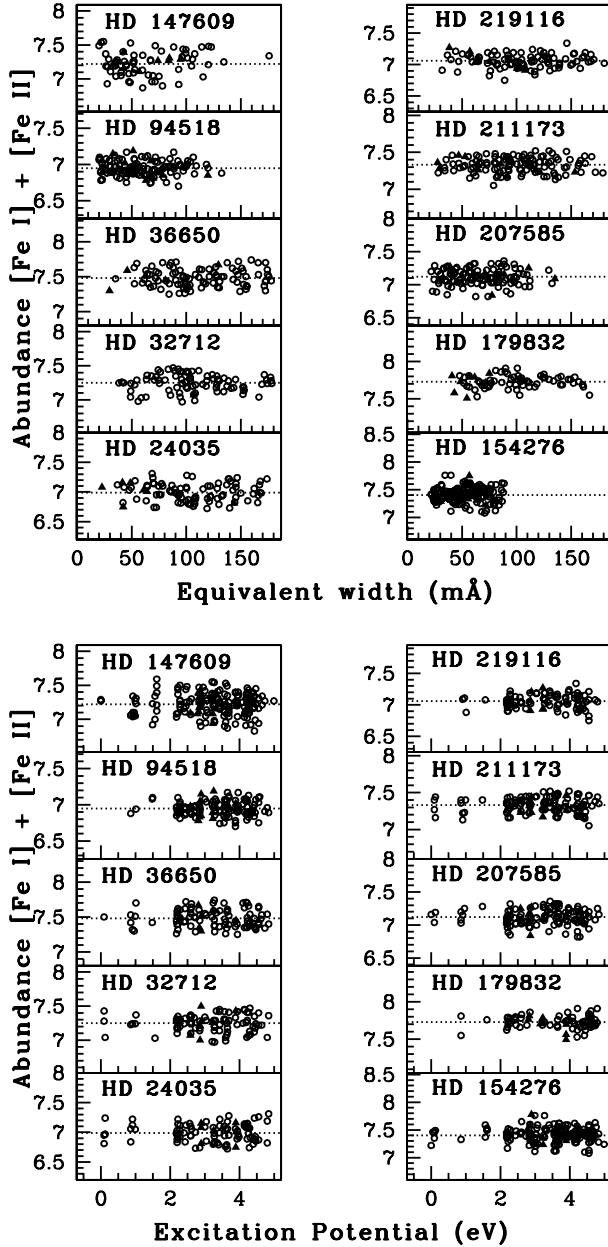


Figure 19. Iron abundances of the program stars for individual Fe I and Fe II lines as a function of Excitation potential (lower panel) and equivalent width (upper panel). Open circles correspond to Fe I and solid triangles correspond to Fe II lines.

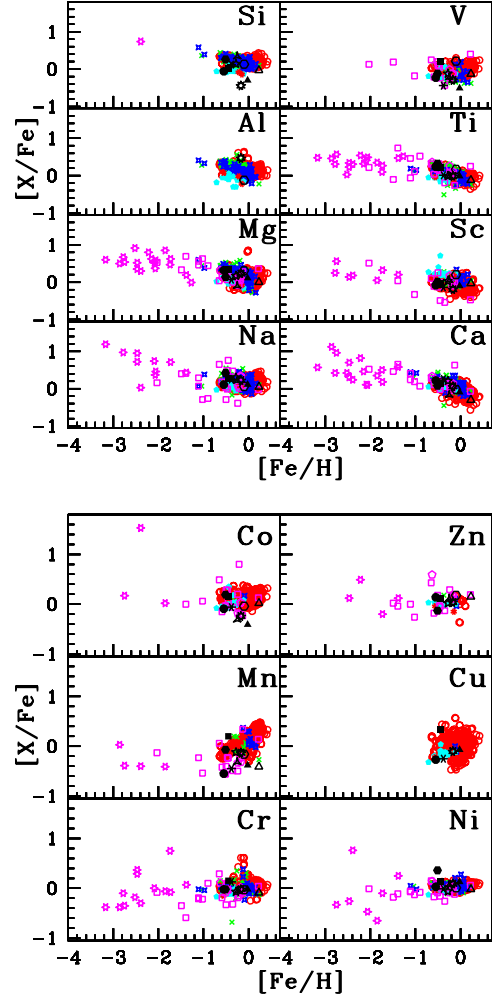


Figure 20. Observed $[X/Fe]$ ratios of the light elements in the program stars with respect to metallicity $[Fe/H]$. Red open circles represent normal giants from literature (Luck & Heiter 2007). Green crosses, blue four-sided stars, cyan filled pentagons, red eight-sided crosses represent strong Ba giants, weak Ba giants, Ba dwarfs, Ba sub-giants respectively from literature (de Castro et al. 2016, Yang et al. 2016, Allen & Barbuy 2006a). Magenta starred triangles represent CEMP stars from literature (Masseron et al. 2010). Magenta open squares and open pentagons represent CH giants and sub-giants respectively from literature (Karinkuzhi & Goswami 2014, 2015, Goswami et al. 2006, 2016, Sneden & Bond 1976, Vanture 1992, Goswami & Aioki 2010, Jonsell et al. 2006, Masseron et al. 2010). HD 24035 (filled hexagon), HD 32712 (starred triangle), HD 36650 (filled triangle), HD 94518 (filled circle), HD 147609 (five-sided star), HD 154276 (open hexagon), HD 179832 (open triangle), HD 207585 (six-sided cross), HD 211173 (nine-sided star) and HD 219116 (filled square).

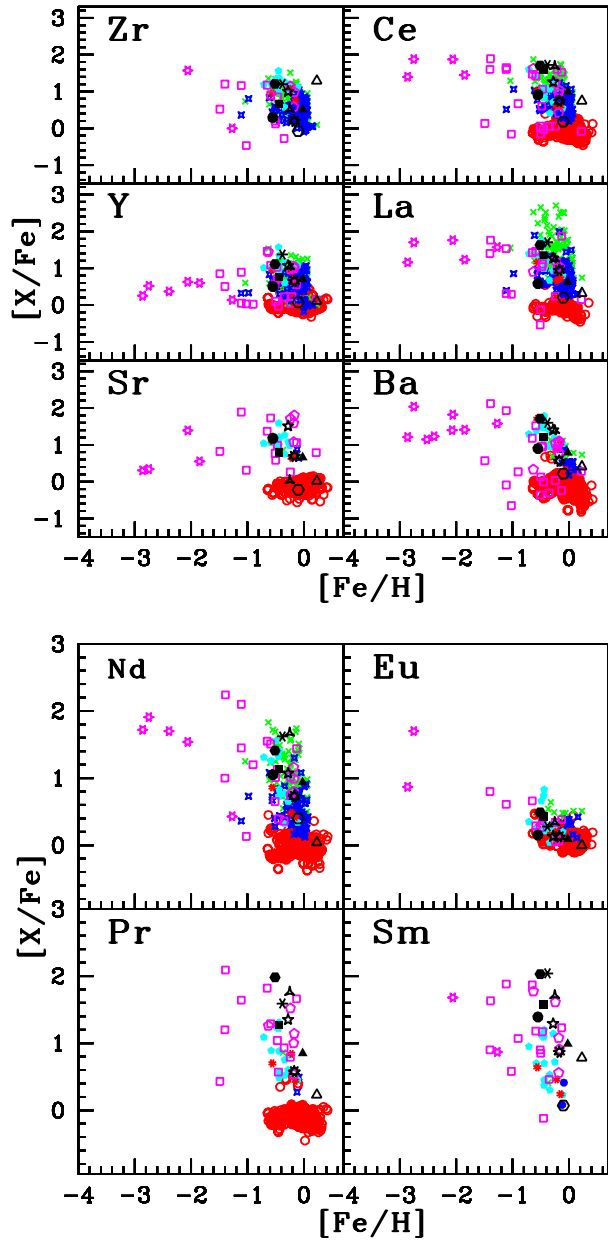


Figure 21. Observed $[X/Fe]$ ratios of heavy elements in the program stars with respect to metallicity $[Fe/H]$. Symbols have same meaning as in Figure 20.